**DNGR-1(+) dendritic cells are located in meningeal membrane and choroid plexus of the noninjured brain**

**TITLE PAGE:**

# DNGR-1+ dendritic cells are located in meningeal membrane and choroid plexus of the non-injured brain.

**Elena Quintana[1a], Andrés Fernández[1a], Patricia Velasco[1], Belén de Andrés[2], Isabel Liste[3], David Sancho[4], María Luisa Gaspar[2] and Eva Cano[1*]**

[1] Neuroinflammation Unit. Unidad Funcional de Investigación de Enfermedades Crónicas, Instituto de Salud Carlos III, Majadahonda, Madrid, Spain.

[2] Department of Immunology. Centro Nacional de Microbiología, Instituto de Salud Carlos III, Madrid, Spain.

[3] Neural Regeneration Unit. Unidad Funcional de Investigación de Enfermedades Crónicas, Instituto de Salud Carlos III, Majadahonda, Madrid, Spain.

[4] Centro Nacional de Investigaciones Cardiovasculares (CNIC), Madrid, Spain.

[a] These authors contributed equally to this work.

**Running title:** DNGR-1/CLEC9A+ dendritic cells in normal brain

**Word count:**

Total: **11941**

Abstract: **218**

Introduction: **630**

Materials and methods: **1473**

Results: **2754**

Discussion: **2576**

References: **1988**

Figure legends including supplemental: **2065**

**Tables:** 2 supplemental tables

**Figure count:** 9 figures and 4 supplemental figures

* **Corresponding Author**

Eva Cano, PhD

Neuroinflammation Unit

Unidad Funcional de Investigación en Enfermedades Crónicas.

Instituto de Salud Carlos III

Carretera Majadahonda-Pozuelo, Km.2,2

Majadahonda-28220, (Madrid) Spain

Phone: +34-91-8223431/432

Fax: +34-91-8223423

Email: ecano@isciii.es

**Main Points:**

**1.-** DNGR-1/CLEC9A is present in mouse brain dendritic cells (bDCs).

**2**.- Brain DNGR-1 expression is enhanced by fms-like tyrosine kinase 3 ligand (Flt3L), a cytokine involved in DC homeostasis.

**3.-** *Dngr-1* mRNA is expressed mainly in the meningeal membranes.and choroid plexus (m/Ch)

**ABSTRACT**

The role and different origin of brain myeloid cells in the brain is central to understanding how the central nervous system (CNS) responds to injury. C-type lectin receptor family 9, member A (DNGR-1/CLEC9A) is a marker of specific DC subsets that share functional similarities, such as CD8α·DCs in lymphoid tissues and $CD103^{+}CD11b^{low}$DCs in peripheral tissues. Here, we analyzed the presence of DNGR-1 in DCs present in the mouse brain (bDCs). *Dngr-1/Clec9a* mRNA is expressed mainly in the meningeal membranes and choroid plexus (m/Ch), and its expression is enhanced by fms-like tyrosine kinase 3 ligand (Flt3L), a cytokine involved in DC homeostasis. Using $Clec9a^{egfp/egfp}$ mice, we show that Flt3L induces accumulation of DNGR-1-$EGFP^{+}$ cells in the brain m/Ch. Most of these cells also express major histocompatibility complex class II (MHCII) molecules. We also observed an increase in specific markers of cDC CD8α+ cells such as *Batf-3* and *Irf-8*, but not of co-stimulatory molecules such as *Cd80* and *Cd86*, indicating an immature phenotype for these bDCs in the non-injured brain. The presence of DNGR-1 in the brain provides a potential marker for the study of this specific brain cell subset. Knowledge and targeting of brain antigen presenting cells (APCs) has implications for the fight against brain diseases such as neuroinflammation-based neurodegenerative diseases, microbe-induced encephalitis and brain tumors such as gliomas.

**TEXT:**

## INTRODUCTION

The immune-privileged state of the brain has received renewed attention in recent years (Galea et al., 2007). Immune cells are today believed to contribute to the physiology of the non-diseased brain, and there is increasing evidence for the existence of distinct cells of myeloid origin in the brain with functions that are still not fully understood (Prinz et al., 2014 and references therein). Brain myeloid cells comprise microglia cells, perivascular, meningeal and choroid plexus macrophages, periphery-derived monocytes, and brain dendritic cells (bDC). Parenchymal microglia is clearly implicated in the steady-state brain. Microglia cells in the healthy brain have a small soma with extensive radial ramifications that actively survey the microenvironment (Nimmerjahn et al., 2005). They have a myeloid origin; they derive from embryonic yolk sac progenitors (Ginhoux et al., 2010) and are sustained by local progenitors (Ajami et al., 2001). A further focus of interest is the trafficking of leukocytes and monocytes through the meningeal and choroid plexus (m/Ch) barrier to patrol the healthy brain or contribute to repair after sterile or non-sterile CNS injury (Ajami et al., 2005; Ransohoff and Cardona, 2010; Shechter et al., 2013).

The existence of dendritic cells in the brain has been described before in non-injured rat and mouse m/Ch (McMenamin, 1999; Matyszak and Perry, 1996; McMenamin et al., 2003), in the EAE (experimental autoimmune encephalomyelitis) mouse model (Serafini et al. 2000; Fischer and Reichmann, 2001; McMahon et al., 2005), and in multiple sclerosis (MS) in the human brain (Prodinger et al., 2011). Recent data obtained with transgenic mouse lines confirm the existence of resident bDCs in the non-diseased mouse brain; for example bDCs from transgenic CD11c-EYFP mice identified by EYFP expression co-localize with other immune markers commonly associated with DCs and microglia/macrophages (Axtell and Steinman, 2009; Bulloch et al., 2008; D'Agostino et al., 2012). Furthermore, bDC $CD11c^{+}$ cells have been

identified in CD11c-GFP mice (Jung et al., 2002; Prodinger et al., 2011). In the periphery, DCs are the antigen presenting cells (APC) that mediate T cell immunity and tolerance. The DC network is complex and comprises several DC subsets, and DC development has been shown to be dependent on fms-like receptor tyrosine kinase 3 ligand (Flt3L) (Heath and Carbone, 2009; Watowich and Liu, 2010). The m/Ch barrier contains a population of Flt3L-dependent DCs akin to the CD8$\alpha^+$ subset of spleen conventional DCs (cDC) (Anandasabapathy et al., 2011). However, further work is needed to precisely characterize the DC subsets in the non-injured brain.

DNGR-1 (CLEC9A) is a C-type lectin receptor that specifically marks a functional subset of DCs defined by dependence on BATF-3, IRF-8 and Id2. Differentiated DCs expressing DNGR-1 include CD8$\alpha^+$ cDCs and CD103+ DCs in peripheral tissues (Huysamen et al., 2008; Iborra et al., 2012; Poulin et al., 2010; Poulin et al., 2012; Sancho et al., 2008; Schraml et al. 2013). DNGR-1 is involved in recognizing death cell antigens (Sancho et al., 2009), and DNGR-1$^+$ DCs could play a role in presentation of antigen to CD4+ T cells and cross-presentation to CD8+ T cells. *Dngr-1/Clec9a* mRNA has been examined in total human and mouse tissues, with the highest expression detected in human brain, thymus and spleen (Huysamen and Brown, 2009), but the specific location of this expression in the brain has so far not been reported. In mouse tissues, different *Dngr-1* isoforms are detected in spleen DCs (Sancho et al., 2008). Here, we analyzed the distribution of brain myeloid cells and the expansion of a DNGR-1$^+$ DC subset after treatment with Flt3L. DNGR-1$^+$ DCs localize in meningeal membranes and choroid plexus (m/Ch) but are scarce in brain parenchyma (BP), and we show that DNGR-1 expression in the brain is increased in response to Flt3L. The tracking of DNGR-1$^+$ DCs will facilitate future studies into the role of this DC subset in the brain.

## MATERIALS AND METHODS

**Cells:** B16 murine Flt3L-secreting tumor cells were grown in DMEM supplemented with 10% FBS (Iborra et al., 2012).

**Animals:** The transgenic mouse line c-fms-EGFP (Csf1r-EGFP) (Sasmono et al., 2003; macgreen), mice expressing EGFP under the promoter of c-fms (CSF1R) are characterized by the expression of enhanced green fluorescence in brain myeloid cells. *Clec9a*$^{egfp/egfp}$ mice (DNGR-1-deficient) (Sancho et al., 2009) on the C57BL/6 background were backcrossed more than 10 times to C57BL/6J-Crl. Batf3$^{-/-}$ mice (Hildner et al., 2008) were backcrossed more than 10 times to the C57BL/6 background and further backcrossed with C57BL/6 mice at the CNIC to establish WT and Batf3$^{-/-}$ colonies from the heterozygotes. Animal studies were approved by the local ethics committee. Mice were bred and maintained in animal facilities at the Instituto de Salud Carlos III. All animal procedures conformed to EU Directive 2010/63EU and Recommendation 2007/526/EC regarding the protection of animals used for experimental and other scientific purposes, enforced in Spanish law under Real Decreto 1201/2005.

**Tissue processing:** For experiments involving immunochemistry, mice were deeply anesthetized by i.p. injection of a mixture of ketamine and xylazine and transcardially perfused with 25-30ml of saline solution for 5 minutes, followed by 4% PFA (Sigma Aldrich, St Louis, MO), pH 7,4, in 0.1M phosphate buffer (PB, Sigma). After perfusion with the fixative, brains were dissected out and post-fixed with 4% PFA for 18-20 h at 4ºC. After fixation, brains were rinsed in 0.1M PB and placed in 15% glucose at 4ºC until they sank, and then in 30% sucrose in PB at 4ºC for 72 hours. Finally, brains were embedded in tissue freezing medium (Tissue-Tek O.C.T$^{TM}$, Sakura), frozen immediately in dry-ice-cooled 2-methylbutane (Sigma-Aldrich), and stored at -70°C. Coronal sections (30 µm) were cut using a CM1950 cryostat (Leica Microsystems) and stored at -20ºC until use. For the CD11c staining, mice were perfused for 1 minute with saline followed by 4% ice-cold PFA and post-fixation for not more than 8 h. The

3D reconstruction in Fig 1s and the meningeal membrane studies were performed with 80 µm vibratome horizontal sections (Leica VT1200s).

**Immunohistochemistry:** Immunohistochemistry was performed on frozen brain sections by standard indirect staining (primary antibody followed by a fluorescent secondary antibody) as described in (Serrano-Perez et al., 2011) but using phosphate as buffer and 10% FBS for blocking. Antibodies were diluted in 0.1M PB containing 1% FBS (Hyclone), 0.06% Triton-X100 (Sigma) and 150 mM glycine (Merck). Rabbit anti-Iba1 (1:100, Wako) was used to detect expression of microglia, Rat anti-mouse I-A/I-E (1:100, clone 2G9, B.D. Pharmingen) was used to detect antigen-presenting cells, Rabbit anti-pan-laminin (L9393 Sigma) was used to detect basal membrane, Rat anti-mouse CD31 (clone MEC13.3 BD Pharmigen) to detect endothelial cells, and biotin-anti-mouse CD11c (clone N418, Biolegend) to detect DCs. Samples stained with CD11c biotinylated antibodies were treated with the Biotin Blocking System (Vector Laboratories) before endogenous peroxidase activity was quenched with hydrogen peroxide. Anti-CD11c staining was detected with horseradish peroxidase-conjugated streptavidin/Cy3-tyramide using the tyramide signal-amplification system (Perkin Elmer, Boston, MA) according to the manufacturer´s instructions. The secondary antibodies used were labeled with Cy3, 488 and 647 fluorochromes (Jackson Immunoresearch). Controls were conducted by omitting the primary antibody, MHC-II controls incorporate the isotype Rat IgG2aκ, and CD11c controls incorporate biotin-control isotype IgG. Slides were finally counterstained with DAPI (5 µg/mL, Life technologies) and mounted in a mixture of Mowiol/50% DABCO (Sigma). Antibodies are described in supplemental Table 1.

**Confocal microscopy and analysis:** Images were acquired on a Leica TCS SP5 inverted confocal laser scanning microscope (Leica Microsystems). Brain maps in Fig 1 were imaged using a 20x objective and a 1.7x digital zoom (4 µm step size, 500 × 500 pixel resolution). Brain maps of smaller areas of Fig 1B (panels a-c) were imaged using a 40x objective and 1.7x digital zoom (2 µm

step size, 500 × 500 pixel resolution). Other images were acquired using a 40× objective (1 µm step size, 1024 × 1024 pixel resolution) for standard images and a 63× objective with a 3x digital zoom (0.5 µm step size, 1024 × 1024 pixel resolution) for detailed images. Images are presented as average projections of z-stacks and keeping parameters constant using negative control slides stained with primary antibody to identify potential non-specific, background fluorescence. Exceptions are mentioned in figure legends. Acquired z-stacks were background-subtracted with Leica LAS AF 2.6.3 software and secondary processed and analyzed using Adobe Photoshop CS3 (Adobe Systems) and ImageJ (National Institute of Health, http://rsb.info.nih.gov/ij) for ROI quantification and cell counting. For 3D reconstructions the plugging 3D viewer for ImageJ was used.

**Cell preparation:** 6–12-wk-old mice with different genetic background as specified were left non-injected or injected subcutaneously (s.c.) in the flank with 5 × $10^6$ B16 murine Flt3L-secreting tumor cells. Between days 12 and 16 after injection, when tumors measured approximately 1 $cm^2$, mice were sacrificed, and intracardiac perfusion was performed using phosphate buffered saline (PBS) with observed blanching of the spleen during 5 min at a speed of 5ml/min. Complete brains and spleens were dissected and for most experiments meningeal (pia-mater) membranes and choroid plexus (m/Ch) were carefully removed with fine tweezers. Brain tissue was finely minced into small pieces and treated with a specific protease mix depending on the tissue. For brain without m/Ch, cells were prepared as in (Sierra et al., 2007) with modifications. Each brain, without the m/Ch and cerebellum, was digested in 5 ml of enzyme solution (20 units/ml papain (Worthington) and 0.025 units/ml DNAse (Sigma) in buffer containing 116mM NaCl, 5.4mM KCl, 26mM NaHCO3, 1mM NaH2PO4, 1.5mM CaCl2, 1mM MgSO4, 0.5mM EDTA, 25mM glucose, and 1mM L-cysteine, pH 7.5) for 30 min at room temperature (RT) with agitation. The brain homogenate was washed and filtered once through a 70-µM filter to remove undigested fragments and then washed twice more, followed by centrifugation at 300g for 7 min. Cells were resuspended in 30% Percoll (GE

Lifesciences) under 5 ml HBSS and centrifuged at 300g for 20min at RT with slow acceleration and no brake. The pellet was collected and washed with HBSS (spin 300g, 7min). All subsequent washes were performed with ice-cold PBS containing 2% (vol/vol) FBS. This preparation contains microglia/macrophage from brain as in Carson et al., 1998, with the exception of those from meningeal membrane, choroid plexus and cerebellum, we refer to this cell preparation as myeloid cells from brain without m/Ch. For m/Ch cell isolates, meningeal membranes plus choroid plexus of at least 3 animals were pooled in an Eppendorf containing 1 ml PBS. Tissue was treated with 2.5 mg/ml pronase (Roche) plus 0.025 units/ml DNase (Sigma) in PBS during 30 min at 37ºC in a bath with mixing. This was followed by homogenization with gentle trituration using glass pipettes until an even homogenate was obtained. m/Ch homogenates were filtered and treated as above. For splenocyte isolation, spleens were mechanically disrupted and teased apart. Cells were collected and ACK (ammonium-chloride-potassium) lysis of red blood cells was followed by two washes and removal of undigested fibrous material by filtering through a 70-um cell strainer. All subsequent steps were performed at 4°C in PBS, 2% FBS.

**Flow cytometry:** Single-cell suspensions were prepared as above and resuspended in staining buffer (2.5% FBS in Dulbecco's PBS; Biowhittaker, Lonza Group). Non-specific binding to Fcγ receptors was blocked with 10 µg/ml of 2.4G2 mAb (Fc block) (BD Biosciences). Staining followed standard protocols, and antibodies and reagents are listed in supplemental Table 1. Fluorochrome-labeled antibodies specific for mouse CD45, CD11b, CD11c, and MHCII were from BD Biosciences or Biolegend. Mouse cell suspensions were incubated with Fc block and were then stained on ice-cold PBS supplemented with 2 mM EDTA, 2% FBS, and 0.02% sodium azide. Cells were analyzed on a FACSCANTO cytometer using FlowJo version 6.3.4 (Tree Star, Ashland, OR).

**RNA isolation, reverse transcription, and real-time PCR:** Total mRNA was isolated with TriPure Isolation Reagent (Roche Applied Sciences, Spain). Total mRNA was quantified and reverse transcribed to cDNA with MMLV

Transcriptase Reverse (Invitrogen), following the manufacturer´s instructions except for the use of 300 ng of random primers and 4 units of RNase OUT (Invitrogen). Semiquantitative PCR of brain and spleen tissues was performed with the AmpliTaq Gold® kit (Applied Biosystems), using 5 ng of total cDNA and 1 μM primers. Spleen samples were loaded at a dilution of 1/30 relative to brain samples to avoid image saturation. The actin primers were forward, GTGGGCCGCTCTAGGCACCAA and reverse, CTCTTTGATGTCACGCACGATTTC. Clec9a/Dngr-1 primers were forward, AGACTGCTTCACCACTCCAA and reverse, CTTGGCACAATGGACAAGGT (Sancho et al., 2008).

Relative amounts of cDNA were analyzed by real-time PCR (RT-PCR) using the FAST SYBR-green system (Applied Biosystems). Each 15 μl reaction volume included 5 ng total cDNA and 0.5 μM of each primer. Mouse 36B4 was used as an internal control to normalize for variation in input RNA. Primers used are as described in supplemental Table 2. The amount of target mRNA in samples was estimated by the 2-ΔΔCT relative quantification method (Livak and Schmittgen, 2001). Ratios were calculated between the amounts of mRNA from the different tissues.

**Statistical analysis:** Statistical analyses were performed using GraphPad Prism 4.0 software. The p values were calculated with the two-tailed Student's *t* test (*p ≤0.05, **p ≤, 0.01, ***p ≤0.001). Data are presented as the means± SEM of a number of experiments (n) indicated in each case.

## RESULTS

### Myeloid cell compartment in the non-injured brain

We first analyzed the myeloid compartment present in the intact brain by confocal microscopy of coronal brain sections from mice expressing the c-*fms*-EGFP reporter construct. The c-*fms* gene encodes the receptor for mouse macrophage colony-stimulating factor (CSF1R/CD115), which in brain is

expressed only in cells of myeloid origin (Sasmono et al. 2003). From hereon we refer to this line as Csf1r-EGFP mice. CSF1R-EGFP$^+$ cells were present throughout the brain in two distinct localizations, the parenchyma itself (BP) and in the perivascular spaces, as shown in (Fig 1A, panel i and ii). CSF1R-EGFP$^+$ cells were found in choroid plexus (Fig 1B panel i and ii) and in the pia mater meningeal membrane (Fig 1C panel i and ii). Interestingly, CSF1R-EGFP$^+$ cells in these localizations have different morphologies: CSF1R-EGFP$^+$ cells in the BP proper have a small soma with extensive radial ramifications and are very evenly distributed throughout the non-injured brain; in contrast, CSF1R-EGFP$^+$ cells in the perivascular areas from the brain parenchyma have a more ameboid morphology with fewer ramifications and were situated in close contact with the basement membrane of brain vessels (Fig 1A, panel ii). CSF1R-EGFP$^+$ cells from choroid plexus were as well brighter, ameboid in shape and they were situated in close contact with CD31$^+$ blood vessels from the plexus as shown in Fig 1B, panel ii. We analyzed the pia mater or pial leptomeniges (meningeal) sliced from the surface of the cerebral hemispheres from the Csf1r-EGFP mouse brains, and observed a dense network of CSF1R-EGFP$^+$ cells that resemble the CD11b$^+$ (OX-42) cells previously described in rat pial leptomeningeal membrane (McMenamin, 1999; McMenamin et al., 2003). To assess the situation of these CSF1R-EGFP$^+$ cells, and to determine if they were situated on top of the pia mater or in the BP, we counterstained with an antibody that recognizes the glial fibrillary acidic protein (GFAP). This antibody stains the glial limitans membrane. In supplemental Fig 1s, we show that the CSF1R-EGFP$^+$ cells constitute a barrier of cells situated in the meningeal membrane above the GFAP$^+$ area. A widely used marker of brain microglia is the ionized calcium binding adapter molecule 1 (Iba1), which recognizes a microglia/macrophage-specific calcium-binding protein (Ito et al., 1998). Analysis of Iba1 expression in non-injured Csf1r-EGFP brains revealed co-expression of Iba1 in 99 ± 0.7 % of CSF1R-EGFP$^+$ cells in BP (supplemental Fig 2s panel A). Iba1$^{low/-}$ CSF1R-EGFP$^+$ cells were very rare in the BP, and the few that we found were next to blood vessels (data not shown). Analysis of m/Ch detected a population of Iba1$^{low/-}$ CSF1R-EGFP$^+$ cells, accounting for 7 ±

2 % of the total CSF1R-EGFP$^{+}$ cells in the choroid plexus (supplemental Fig 2s panel B). We could not observe Iba1$^{+}$ cells that were CSF1R-EGFP$^{-}$. To analyze Iba1$^{+}$ and CSF1R-EGFP$^{+}$ in the meningeal (m) membranes we used 80μm horizontal vibratome sections, choosing the very first slide from the brains. In this brain localization, we observed CSF1R-EGFP$^{+}$ cells that were clearly Iba1$^{low/-}$ (supplemental Fig 2s panel C); in fact, most of the very bright CSF1R-EGFP$^{+}$ located in the pia leptomenigeal membrane were Iba1$^{low/-}$, and we could only see Iba1$^{+}$ CSF1R-EGFP$^{+}$ cells in the proper brain tissue.

To further analyze brain myeloid cells we isolated CD45$^{+}$ cells from the brain without (w/o) m/Ch preparations and m/Ch of Csf1r-EGFP mice; the gating strategy used to exclude dead cells and doublets is presented in supplemental Fig 3s. Cells of ectodermal origin, such as astrocytes, oligodendrocytes and neurons, which together with endothelial cells constitute the majority of cells in the brain, are not labeled with CD45 antibodies. Therefore, due to the lack of specific markers for microglia itself, we used CD45 expression to characterize the proper microglia, which have a medium expression of CD45 (CD45$^{m}$), and myeloid cells from the periphery as CD45 high (CD45$^{h}$) (Carson et al., 1998; Ford et al., 1995). CD45$^{+}$ cells accounted for 30 to 40% of total live cells in brain w/o m/Ch isolates (Fig 2A panel i-iv), and 20 to 30% of cells obtained from m/Ch preparations (Fig 2B panel i-iv). The percentage of CD45$^{+}$ cells obtained was similar in wild type (WT) and Csf1r-EGFP mice. In isolates from Csf1r-EGFP mice, ≥ 96% of cells were CSF1R-EGFP$^{+}$ CD45$^{+}$ (Fig 2A, B). We found few CD45$^{+}$ EGFP$^{-}$ cells in the brain w/o m/Ch cell isolates (Fig 2A panel v) and in the m/Ch preparations (Fig 2B, panel v). To include this small CSF1R-EGFP$^{-}$ CD45$^{+}$ subset in our study, we used CD45 labeling instead of EGFP expression to study brain myeloid cells for subsequent analysis.

**Flt3L-dependent accumulation of CD45$^{+}$ cells in brain**

We are interested in the different myeloid cell subsets present in the steady-state brain. In this context, an increase in bDC numbers has been

reported after treatment of mice with Flt3L (Greter et al., 2005; Anandasabapathy et al., 2011). The latter authors observed an increase in a $CD45^{h}CD11c^{+}MHCII^{+}$ cell population that was expanded after treatment of mice with Flt3L. We isolated brain myeloid cells from untreated (-Flt3L) and Flt3L treated (+Flt3L) WT animals and analyzed $CD45^{+}$ cell numbers. In brain w/o mCh preparations we distinguished two $CD45^{+}$ populations according to fluorescence intensity in response to FLT3L, and in accordance with published data (Carson et al., 1995) we refer to these as $CD45^{m}$ (medium intensity) and $CD45^{h}$ (high intensity) (Fig 3). Flt3L treatment did not increase the percentage of total $CD45^{+}$ cells isolated (Fig 3A panel I). However, Flt3L treatment did increase the frequency and numbers of cells in the $CD45^{h}$ population in isolated cells from brain w/o m/Ch (Fig 3A panel II and 3C). The Flt3L-induced increase in the BP $CD45^{h}$ subpopulation prompted us to analyze if these cells were of myeloid origin. For this analysis we detected the marker CD11b, also known as Integrin alpha M chain (ITGAM), in an approach similar to that used in rat by (Ford et al., 1995). Three subpopulations were detected in BP. The largest (69 ± 7% of $CD45^{+}$ cells) was $CD45^{m}CD11b^{+}$ (Fig 3B); these cells correspond to brain microglia based on their medium staining with the CD45 marker and their staining with the CD11b marker. The other two subpopulations subdivide the $CD45^{h}$ population according to CD11b expression: $CD45^{h}CD11b^{+}$ (15 ± 4%) and $CD45^{h}CD11b^{low}$ (15 ± 5%), and correspond to blood-borne cells as described by using irradiation chimeras (Ford et al., 1995).

Similar analyses were performed in m/Ch cell preparations (Fig 4). The percentage of $CD45^{+}$ cells was 32 ± 6% in the absence of Flt3L, increasing to 44 ± 6% upon Flt3L treatment in these brain localizations. The numbers of isolated $CD45^{+}$ cells varied between the untreated and Flt3L-treated groups (Fig 4A, panel I). CD45 and CD11b marker expression distinguished only two subpopulations: $CD45^{h}CD11b^{+}$ (66 ± 2%) and $CD45^{h}CD11b^{low}$ (26 ± 1%) (Fig 4B). The percentage and numbers of total $CD45^{+}$ cells obtained from m/Ch was not significantly affected by Flt3L treatment, but the relative frequency and numbers of $CD45^{h}CD11b^{low}$ cells was increased (Fig 4A panel II and 4C). The

number of $CD45^{h}CD11b^{low}$ cells was 82 ± 15 cells/$10^3$ $CD45^+$ cells, increasing approximately 3-fold to 261 ± 11 cells/$10^3$ $CD45^+$ cells in the presence of Flt3L (Fig 4C).

bDCs have been identified mainly in the m/Ch (see Introduction). Flt3L-responsive m/Ch cells in the brain have been reported to have a $CD45^{h}CD11c^{+}MHCII^{+}$ phenotype, detected mainly with the use of the CD11c-EYFP transgenic mouse (Anandasabapathy et al., 2011). Using our m/Ch brain isolation methodology, we were unable to detect $CD11c^+$ cells in our flow cytometry (FC) analyses, although the antibody was able to recognize the presence of $CD11c^+$ cells in the spleen (supplemental Fig 4s and Discussion). Since bDCs should express major histocompatibility complex class II (MHCII) antigens in their membrane, we first analyzed the expression of MHCII by immunofluorescence (IF). $MHCII^+$ cells were rarely found in the BP, but when found they were situated always in close proximity with blood vessels (Fig 5A). $MHCII^+$ cells in the Flt3L treated mice were mainly situated in the plexus (Fig 5B). Most of the cells analyzed showed co-localization of both markers, although we noted that stronger staining of the MHCII antigen corresponded to a less bright CSF1R-$EGFP^+$ fluorescence by IF (not quantified) (Fig 5B, panel ii). In the pia leptomeningeal membrane, most CSF1R-$EGFP^+$ cells were $MHCII^-$ (Fig 5C, panel i), and when $MHCII^+$ cells were found, they were situated close to vessels and in clusters (Fig 5C, panel ii inset). These $MHCII^+$ cells in meningeal membrane showed a diminished EGFP fluorescence (Fig 5C, panel ii), and were seen only in Flt3L-treated mice.

We wanted to analyze the presence of $CD11c^+$ in the non-injured mice without using transgenic mice such as the CD11c-YFP (Bulloch et al., 2008) or CD11c-GFP (Prodinger et al., 2011). For this purpose, we analyzed Flt3L-treated animals to increase the number of these cells and used a Tyramide Signal Amplification (TSA) method in combination with our Alexa Fluor dyes to achieve high-resolution signal amplification as specified in material and method section. Following this protocol we have been able to observe $CD11c^+$ cells in the m/Ch but not in the BP. These $CD11c^+$ cells were more numerous in the

plexus, and they co-localized with MHCII staining as shown in Fig 5D. To be able to analyze in more detail $MHCII^+$ in the different brain localization, we analyzed cell suspensions isolated from brain w/o mCh (Fig 6A) and m/Ch preparations (Fig 6B). Cells from the BP of untreated control animals (-Flt3L) had a $CD45^m$ phenotype, and FC analysis showed that these cells were $MHCII^-$. Flt3L treatment induced MHCII expression in less than 1% of cells in this $CD45^m$ subpopulation (Fig 6A, panel I). The $CD45^hCD11b^+$ population contained 36 ± 5% $MHCII^+$ cells, and this percentage did not vary significantly in the presence of Flt3L (41 ± 7%) (Fig 6A, panel II). The amount of $CD45^hCD11b^{low}$ cells obtained in the non-injured brain varied between different brain preparations. The majority of these cells (79 ± 7%) expressed MHCII in their membranes (Fig 6A, panel III). Since we did not observe $MHCII^+$ cells in the parenchyma proper by IF analysis, we believe that these $MHCII^+$ cells might reflect contamination by m/Ch cells or perivascular myeloid cells. Further analysis is required to assess the localization and origin of these $MHCII^+$ cells in the brain parenchyma.

When m/Ch preparations were analyzed, we observed a 3-fold increase in the number of $CD45^hCD11b^{low}$ cells, as shown before (Fig 4). Of the $CD45^hCD11b^{low}$ cells obtained from m/Ch, 70 ± 3% were $MHCII^+$ (Fig 6B). In conclusion, Flt3L treatment preferentially expands a $CD45^hCD11b^{low}$ subset of $MHCII^+$ cells in the m/Ch. The fact that these cells are increased in the presence of Flt3L and that they have a $CD45^hCD11b^{low}MHCII^+$ phenotype leads us to think that they are the bDCs previously described in m/Ch (Anandasabapathy et al., 2011; McMenamin, 1999; McMenamin et al., 2003; Prodinger et al., 2011), and that we detected localized mainly in the choroid plexus (Fig 5).

**Expression of *Dngr-1* transcripts in mouse brain**

The gene expression profile of Flt3L-responsive m/Ch myeloid cells bears strong similarities to that of the CD8α+ DC subpopulation in the spleen (Anandasabapathy et al., 2011). The high expression of DNGR-1 (CLEC9A) is

an excellent marker of Batf3-IRF8-Id2-dependent DCs of the CD8α+ family (Caminschi et al., 2009; Huysamen et al., 2008; Sancho et al., 2008); reviewed in (Shortman and Heath, 2010). We expanded DNGR-1$^+$ DCs by treatment with Flt3L (Iborra et al. 2012) and analyzed *Dngr-1*mRNA expression in spleen (positive control) and in an array of brain structures: olfactory bulb (Ob); cerebellum (Cbl); brain cortex (Ctx); striatum (Str); meningeal membranes and choroid plexus (m/Ch); subventricular zone (SVZ) isolated as in (Ferron et al., 2007; Guo et al., 2012); hippocampal formation (Hpp) and thalamus (Th). Only the m/Ch samples showed expression of all DNGR-1 isoforms (Fig 7A and 7B), similarly to the defined isoforms in the mouse spleen (Sancho et al., 2008). As a control of specificity, we used spleen and brain tissue from untreated and Flt3L-treated *Clec9a*$^{egfp/egfp}$ mice, which lack DNGR-1, confirming no amplification of the specific *Dngr-1* transcript in these samples (data not shown).

Selective expression of *Dngr-1* in m/Ch of Flt3L-treated animals was corroborated by real time PCR. The higher sensitivity of this technique allowed detection of *Dngr-1* transcripts in the BP, but in lower amounts than in m/Ch. Flt3L strongly augmented the amount of *Dngr-1* transcript in splenocytes and m/Ch preparations, with the expression of *Dngr-1* in Flt3L-treated splenocytes around 5 times higher than in m/Ch cell preparations (Fig 7C). This Flt3L-triggered increase in the expression of *Dngr-1* is consistent with the increase in the percentage of CD45$^h$ cells induced by the same cytokine (Fig 3 and 4). Together, these results show that Flt3L induces *Dngr-1* expression preferentially in the m/Ch.

The procedures for isolating cell populations from the adult brain expose cells to enzymes and mechanical forces that can damage membranes or membranes molecules. Some of these enzymatic procedures could cleave specific membrane cellular markers of interest such as DNGR-1, leading to false negative results in the FC analysis. To circumvent this problem, we used *Clec9a*$^{egfp/egfp}$ mice (Sancho et al., 2009), which express a farnesylated form of EGFP in frame with the first two aminoacids of DNGR-1. Thus, expression of EGFP marks DNGR-1-expressing cells, and is restricted in the spleen to CD8α$^+$

cDC cells (Sancho et al., 2009). Accordingly, Flt3L treatment induced a 10-fold expansion of EGFP$^+$ DCs in the spleen (supplemental Fig 3s). Cytometry analysis of BP and m/Ch cells isolated from ±Flt3L-treated WT and *Clec9a*$^{egfp/egfp}$ mice revealed EGFP expression in CD45$^h$ cells in both cell preparations. In BP there was a modest but significant increase in the numbers of CD45h EGFP$^+$ cells (Fig 8A), whereas in m/Ch preparations the CD45$^h$ EGFP$^+$ cells were increased 10-fold by Flt3L treatment (Fig 8B).

We next analyzed the expression of MHCII antigen in EGFP$^+$ cells. As a positive control, we analyzed the Flt3L-induced increase in EGFP$^+$ splenocytes, finding that all CD45$^+$ DNGR-1-EGFP$^+$ cells in the spleen were MHCII$^+$ (supplemental Fig 4s panel B). Analysis of brain w/o m/Ch and m/Ch isolates showed that DNGR-1-EGFP$^+$ cells were also MHCII$^+$ in the brain by FC analysis (Fig 9A and B). EGFP$^+$ cells have low expression of CD11b, and correspond to the CD45$^h$CD11b$^{low}$ subpopulation described in Fig 3 and Fig 4. Since MHCII$^+$ cells in Flt3L-treated animals are situated mainly in the choroid plexus (Fig 5), we analyzed if the DNGR-1-EGFP$^+$ cells were positive for CD11c and MHCII, both known DC markers (see Introduction). DNGR-1-EGFP$^+$ cells were localized mainly in the plexus and were detected by a weak direct fluorescence of EGFP protein. These DNGR-1-EGFP$^+$ cells co-expressed the MHCII and CD11c markers (Fig 9C). These findings thus establish the existence of a subset of CD11c$^+$ MHCII$^+$ cells that express DNGR-1 in the brain. Our conclusion is that DNGR-1 expression allows for further discrimination of DC subsets in the brain.

The surface protein and mRNA expression analyses performed here indicate that the majority of Flt3L-dependent cells in the brain are located in the m/Ch. To confirm the DC-nature of the Flt3L-dependent cell population in the m/Ch, we analyzed the mRNA expression of DC molecular markers typical of DNGR-1$^+$ DCs (Poulin et al., 2010; Poulin et al., 2012) by quantitative RT-PCR. Choroid plexus from Flt3L-treated mice showed increased mRNA expression of the transcription factors *Irf-8* (interferon regulatory factor 8) and *Batf-3* (basic leucine zipper transcription factor ATF-like 3) (Fig 9E). We also detected

increased expression of *Cd103* (integrin alpha E (ITGAE)) a molecule expressed in dendritic cells from non-lymphoid tissues (reviewed in del Rio et al., 2010). In contrast, mRNAs encoding the co-stimulatory molecules *Cd40 (*data not shown), *Cd80* and *Cd86* were not increased after Flt3L treatment, consistent with non-activated state of these DCs in the normal brain. These results thus indicate that Flt3L-treated m/Ch show increases in the expression of genes that specifically mark the splenic CD8$\alpha$+ DC and peripheral CD103$^+$ DC subsets, and therefore the bDCs described here share similarities with this specific DC subset.

Deletion of the transcription factor Batf3 has been shown to ablate development of CD8α$^+$ DCs in the periphery (Hildner et al., 2008). We therefore predicted that the m/Ch of mice lacking this transcription factor (Batf3$^{-/-}$) would be defective for Flt3L accumulation. Flt3L-treated Batf3$^{-/-}$ animals did not show increases in *Dngr-1* mRNA when compared with similarly-treated wild type littermates (Fig 9E). This implies that Flt3L-induced DNGR-1-EGFP$^+$ CD11c$^+$ MHCII$^+$ cells in the brain are very similar and have the same requirements as their peripheral CD8α$^+$ DC counterparts. The exact role of these cells in the intact and injured brain remains to be defined.

## DISCUSSION

In the present study we have shown Flt3L-dependent accumulation of a population of DNGR-1(CLEC9A)-EGFP$^+$ CD45$^h$ CD11b$^{low}$ MHCII$^+$ myeloid cells in the brain. These cells accumulate mainly in the m/Ch that surrounds the brain. We call these cells m/Ch DCs, as has been proposed before (Anandasabapathy et al., 2011). These cells have been shown to share functional and developmental characteristics with CD8$\alpha^+$ cDCs from spleen, and here we show that m/Ch DCs express the C-type lectin receptor DNGR-1/CLEC9A.

The entry and activation of T cells in the brain parenchyma requires a preexisting interaction of these cells with APCs. Most cells in the body can present antigen to CD8$\alpha^+$ T cells via MHC class I molecules, and thus act as APCs. However, the term APC is often reserved for specialized cells that can prime $CD8^+$ (cytotoxic) T cells through MHC class I molecules and also stimulate $CD4^+$ (helper) T cells through MHC class II. APCs that express MHC class II molecules are often called professional APCs, and mainly consist of macrophages and dendritic cells. To isolate brain myeloid cells which express MHCII in their membranes, and therefore can function as professional APCs in the brain, we made use of Csf1r-EGFP mice (Fig 1 and 2), which express EGFP protein under the control of the CSF1R/CD115/fms promoter (Sasmono et al., 2003). CSF1R plays an important role in the development and maintenance of brain microglia (Elmore et al., 2014; Erblich et al., 2011), and our data show the existence of morphologically distinct CSF1R-$EGFP^+$ cells in BP and m/Ch of Csf1r-EGFP mice (Fig 1). These data are in line with previously described results showing myeloid cells from non-injured rat and mouse brains, identified with an array of different antibodies and methods (Bulloch et al., 2008; Matyszak et al., 1992; McMenamin, 1999; McMenamin et al., 2003; Prodinger et al., 2011). The use of a well-known marker for brain microglia cells such as Iba-1 showed that in the brain tissue this cellular marker co-localizes with CSF1R-$EGFP^+$ in the IF analyses (Fig 2s). These results show that CSF1R-EGFP transgenic mice reproduce the morphological difference between the distinct myeloid cells existing in the brain. We could detect two different myeloid cells in the brain: the microglia proper, with small soma and long prolongations as described in the literature (see Introduction), and more ameboid cells in close proximity to the vessels, which might correspond to perivascular macrophages, as observed before (Prodinger et al., 2011). Although these authors reported a population of CD11c-$GFP^+$ cells in this location, we could not observe $CD11c^+$ cells by IF analysis. Most of the CSF1R-$EGFP^+$ cells isolated from non-injured BP showed moderate expression of CD45 ($CD45^m$), with very few $CD45^h$ expressing cells, a finding in accord with the low frequency of infiltration by peripheral leukocytes in the healthy brain (Ginhoux et al., 2009;

Mildner et al., 2007). Our isolation methods are based on those described by other authors (Carson et al., 1998; Ford et al., 1995), and in agreement with their data, our isolation procedure with long perfusion of the brains before isolation eliminate most of the $CD45^{h}$ cells from the BP preparations. It is still possible that this isolation method does not efficiently extract these perivascular cells, and that we are therefore not evaluating the exact number of these $CD45^{h}$ cells in the FC analysis. Further work will be required to clarify the number of $CD45^{h}$ cells residing in the perivascular space and determine to what extent they are induced by Flt3L.

In cells obtained from the m/Ch, 4 ± 3% of isolated $CD45^{+}$ cells were CSF1R-$EGFP^{-}$ by FC. These cells are of myeloid origin, since they were labeled with anti-CD11b antibody. The use of the Csf1r-EGFP mice together with IF with other well-known myeloid markers reveals the complexity of the myeloid cells in the brain. We observed a variation in the intensity of CSF1R-$EGFP^{+}$ staining, and since 7 ± 2% of the CSF1R-$EGFP^{+}$ cells we detected were $Iba1^{low/-}$ in the m/Ch preparations, this suggests that different myeloid cells coexist in the normal brain. As yet we do not know the exact origin of these cells, or if they differ functionally from the CSF1R-$EGFP^{+}$ $Iba1^{+}$ cells. CSF1R-$EGFP^{+}$ $Iba1^{-}$ cells were very prominent in the meningeal membrane, and future studies will need to analyze the choroid plexus and meningeal membrane separately. We are currently studying how these cell populations change in response to neuroinflammatory challenges. So far, our data suggest that more than one myeloid-specific marker might be required to give a clear picture of the number and complexity of myeloid cells in the brain, particularly in the brain membranes and choroid plexus, and that analyses by cell suspension FC and IF will be required.

Flt3L treatment did not increase the numbers of CSF1R-$EGFP^{+}$ cells in brain isolates or m/Ch compartments (data not shown). This finding is in accordance with previous data showing that Flt3L-responsive m/Ch DCs express the Flt3L receptor but not the CSF1R/CD115 receptor on their cell surface (Anandasabapathy et al., 2011). Our data show that, while the Csf1r-

EGFP mouse is a good model for visualizing microglia cells in the brain, there is a subset of myeloid cells that we might be overlooking. For this reason we carried out most of our brain myeloid analysis on $CD45^{+}$ cells, distinguishing the $CD45^{m}$ resident microglia cells in the BP from $CD45^{h}$ myeloid cells of peripheral origin. Although we did not confirm this observation in mouse-chimera experiments, this distinction between resident and peripheral-origin $CD45^{+}$ cells in the brain has been observed by many studies of microglia and peripheral infiltrating brain macrophages (Anandasabapathy et al., 2011; Ford et al., 1995).

These results raise the question of whether these Flt3L-dependent cells are true dendritic cells. The existence of brain parenchymal dendritic cells in the normal brain is still debated, although cells with DC markers have been found in various CNS locations (Matyszak et al., 1992; Matyszak and Perry, 1996; McMenamin, 1999; McMenamin et al., 2003). More recently, the presence of $CD11c^{+}$ cells have been described through the use of transgenic mice such as the CD11c enhanced yellow fluorescent protein (EYFP) model, which was constructed to identify dendritic cells in the periphery (Lindquist et al., 2004), and in CD11c-GFP mice (Jung et al., 2002). The analysis of these transgenic mice showed CD11c-fluorescent cells residing mainly in the m/Ch, the perivascular spaces and juxtavascular parenchyma, with the entire population of CD11c-$EYFP^{+}$ cells co-expressing Iba1 and MHCII in the steady-state brain parenchyma (Anandasabapathy et al., 2011; Bulloch et al., 2008; Prodinger, et al., 2011). Previous work has shown the presence of MHCII+ cells in the m/Ch but not in BP from non-injured rat and mice brain by IF analysis (Matyszak et al., 1996), in line with our results. Many more studies have described an increase in these MHCII+ cells under neuroinflammatory conditions (Lv et al., 2011; Prodinger et al., 2011; Greter et al., 2005). Our analysis of the non-injured brain shows clear expression of $MHCII^{+}$ cells in m/Ch, and we expected that these cells would express CD11c. In their study, Bulloch et al. discuss the difficulty in identifying CD11c protein in young, steady-state brains with the antibodies available, which were found to be unreliable and give inconsistent

results in confocal microscopy analyses. These results are in line with previous reports (Fischer and Reichmann, 2001; Greter et al., 2005; Karman et al., 2006; Matyszak and Perry, 1996; McMenamin, 1999) in which DCs were detected with the same antibodies in the setting of neuroinflammation but very rarely in the non-injured brain (reviewed in (Pashenkov et al., 2012; Ranshohoff, 2012). The use of transgenic mice such as CD11c-YFP and CD11c-EGFP has been very useful to visualize $CD11c^+$ cells in non-injured mice, although the use of DT in CD11c-DTR-GFP mice did not exclusively lead to depletion of DCs, but also targeted macrophages in various tissues (Probst et al., 2005; van Rijt et al., 2005). Here, we used a tyramide-based method to enhance positive staining with the CD11c antibody. $CD11c^+$ cells in the non-injured brain were studied in Flt3L-treated mice, and were found mainly in the choroid plexus. Using these methods we clearly show the presence of $CD11c^+$ cells in the undamaged brain, although the combined use of other molecular markers such as MHCII might provide a way to detect more accurately the presence of myeloid cells with a potential role as APCs. As we show in the non-diseased brain (Fig 5), $MHCII^+$ cells are present mainly in the brain choroid plexus in our brain preparations, although Flt3L induced the presence of MHCII+ in the meningeal membrane close to blood vessels (Fig 5C). In accordance with previous published work in rat brain (Matyszak et al., 1992; McMenamin, 1999; McMenamin et al., 2003), $MHCII^+$ cells are very prominent in the brain membranes, mainly in the choroid plexus, but very rare in the BP. We detected some but not many $MHCII^+$ cells near the vessels, in close proximity to the basement membrane (Fig 5A), but were unable to detect $CD11c^+$ cells in the perivascular or juxtavascular area as shown in (Prodinger et al., 2011). High background around bigger vessels in the brain parenchyma made it difficult to visualize $CD11c^+$ cells in this brain localization (data not shown). We did not observe this background around vessels in m/Ch preparations (Fig 5)

As we mentioned before, we have thoroughly tried to analyze the presence of this marker in our preparation by FC analyses, without success. Our failure to detect CD11c by FC analysis might be explained in part by the

susceptibility of membrane markers to digestion with the proteases used in the cell preparation protocol. Very recently (Immig et al., 2015), a very weak CD11c staining of brain myeloid cells has been shown by FC; these authors obtained their brain preparation without proteases, and this technique should be taken into account in future FC analysis of $CD11c^{+}$ cells in the uninjured brain.

The results presented here were generated in the non-injured mouse brain, with no neuroinflammatory trigger. In line with the literature (Carson et al., 1998), our data indicate that BP contains a low percentage of $CD45^{h}$ cells in this condition. Nevertheless, we consistently observed that Flt3L treatment increased the number of $CD45^{h}$ cells in the BP preparation (Fig 3), which contains few MHCII cells (Fig 5). Our IF analysis with anti-MHCII antibodies barely detected any $MHCII^{+}$ cells in the brain parenchyma itself (Fig 5), and those that were present were situated in contact with blood vessels (Fig 5A). In this context, Iming et al., 2015 show a lack of MHCII staining in their CD11c-positive microglia cells. Our CD11c analyses by IF did not show any $CD11c^{+}$ cell in the parenchyma when the CD11c+ cells in the m/Ch were neatly observed. It is still possible that since the mean of fluorescence (MFI) in microglia is lower that might well be below the detection threshold of the technique used in these studies.

At present, we cannot discard the possibility that the Flt3L-enhanced presence of $CD45^{h}$ $MHCII^{+}$ BP cells in the FC analysis might reflect contamination by m/Ch membrane cells. In m/Ch, we observed a Flt3L-triggered increase in the percentage of $CD45^{h}$ $CD11b^{low}$ $MHCII^{+}$ cells, which corresponded to the number of $MHCII^{+}$ cells observed by IF (Figures 5 and 6). Our findings are thus in accordance with previous data indicating the absence of $MHCII^{+}$ cells in the BP proper of the non-diseased young brain and their localization in the m/Ch (Greter et al., 2005; Lv et al., 2011; Prodinger et al., 2011; Puntener, 2012). Further combined analysis by FC and IF with an array of different cellular markers will shed new light on the phenotype, activation stage and role of brain myeloid cells in the response to diverse neuroinflammatory stimuli.

There is an emerging role for DNGR-1$^+$ cells in the induction of T cytotoxic cell responses to cancer, viruses and other pathogenic infections. In the brain, Piva et al. reported that depletion of DNGR-1-positive cells decreases the number of CD8+ T cells in the brain after induction of experimental cerebral malaria (Piva et al., 2012). Here, we have shown a clear accumulation of DNGR-1-EGFP$^+$ cells in the Flt3L-treated m/Ch (Fig 8). Moreover, these cells are enriched in *Dngr-1* mRNA, (Fig 7) and there is a parallel increase in the numbers of MHCII$^+$ cells (Figures 6 and 8). We also observed a very dull fluorescence of DNGR-1-EGFP$^+$ cells in the m/Ch, but not in BP (data not shown). In fact, we could not clarify whether DNGR-1$^+$ cells are present in the BP. On one hand, RT-PCR analysis detected a weak but significant increase in *Dngr-1* mRNA expression in response to Flt3L (data not shown) and an increase in the number of Flt3L-dependent DNGR-1-EGFP$^+$ cells in the BP (Fig 8A). On the other hand, our immunofluorescence analysis did not detect MHCII$^+$ cells in the BP. Therefore, it seems likely that the DNGR-1-EGFP$^+$ and MHCII$^+$ cells detected by FC in BP preparations reflect contamination by membrane structures during dissection.

The relationship between mouse CD8$\alpha^+$ DCs from lymphoid tissues and CD103$^+$CD11b$^{low}$DCs from non-lymphoid tissues has been established (Ginhoux et al., 2009). These cells and their human counterparts all express the DNGR-1 receptor (Poulin et al., 2012). CD8$\alpha^+$ peripheral DCs have been implicated in the homeostatic maintenance of immune tolerance and the prevention of autoimmune disease. Furthermore, in spleen, CD8$\alpha^+$ DNGR-1/CLEC9A DCs share with other DCs the ability to process and present antigens in the context of MHC class II, but are more efficient in the phagocytic uptake of dead cells (Inaba et al., 2002; Iyoda et al., 2002; Schulz and Reis e Sousa, 2002). Indeed, DNGR-1 has been identified as a receptor able to recognize cell-death antigens and is a dedicated receptor for cross-presentation of cell-associated antigens (Pooley et al., 2001; Zelanay et al., 2012). Characterizing the exact role of these cells accumulating in the brain in the presence of Flt3L will be an interesting subject to pursue in the coming years.

Our results support a dendritic-like nature for Flt3L-dependent cells in the brain. First, they are responsive to Flt3L, a cytokine that has been shown to increase the dendritic repertoire. Second, they express DNGR-1, indicated by examination of *Cle9a*$^{egfp/egfp}$ mice and the expression of *Dngr-1* mRNA. Finally, they express the transcription factors Batf-3 and Irf-8, both of which are required for the maturation of CD8α$^{+}$ classical DCs (Murphy, 2013). Although the presence of MHCII on the membrane is a requisite for antigen presentation, it is not sufficient to obtain a full T cell activation. CD80 and CD86 are co-stimulatory molecules that have an important role for antigen-presentation to T-cells. In presence of Flt3L we have not observed an increase in the mRNA levels of these molecules in the mCh despite the Flt3-L dependent increase in MHCII$^{+}$ cells (Fig 9B). Therefore, our data so far do not clarify whether these cells are efficient in their role as antigen-presenting cells or if extra signals are required to achieve a mature DC phenotype. Since we have not observed an increase in the co-stimulatory molecules, we hypothesize that these cells do not efficiently activate T cells, and that an extra neuroinflammatory signal is required. We are currently analyzing what signals are required to obtain a full immune response in these cells.

The existence, regulation and role of APCs in the brain DCs has implications for the development of strategies to target cargoes to these m/Ch brain DCs using receptor-specific antibodies. The expression of the highly specific receptor DNGR-1 in these cells makes such strategies especially attractive The similarity of these cells to lymphoid CD8α$^{+}$DNGR-1$^{+}$ cells suggests that they might be responsible for producing efficient CTL responses (Caminschi et al., 2008; Sancho et al., 2008), and therefore could be an important target in brain disorders such as neuroinflammation-based neurodegenerative diseases, microbe-induced encephalitis and brain tumors such as gliomas.

**Acknowledgments:** We thank David Hume (The Roslin Institute, University of Edinburgh) for providing the c-fms/Csf1r EGFP mice. Batf-3$^{-/-}$ was kindly provided by Dr. Kenneth M. Murphy, Washington University, St. Louis, MO, USA. We thank Amanda Sierra (Universidad del Pais Vasco) for her scientific discussions. Simon Bartlett (CNIC) provided English editing. This work was supported by grants PI09/0218 and PI12/0238 from the Fondo de Investigaciones Sanitarias (FIS) Spain to E Cano and by grant RD12/0036/0027 from the Red Temática Investigación Cooperativa en Cáncer (RTICC).

**Abbreviations: CNS**: central nervous system; **BP:** brain parenchyma; **m/Ch**: meningeal membranes and choroid plexus; **EGFP**: enhanced green fluorescent protein; **CSF**: colony-stimulating factor; **CSF1r**: colony-stimulating factor 1 receptor; **FLT3-L**: FMS-like tyrosine kinase 3 ligand; **Iba1**: ionized calcium-binding adapter molecule 1; **MHC**: major histocompatibility complex; **GFAP:** glial fibrillary acidic protein; **DNGR-1/ CLEC9A**: C-type lectin domain family 9, member A; **APC**: antigen presenting cell; **DC**: dendritic cells; **bDC:** brain dendritic cells; **CTL**: cytotoxic T lymphocyte; **FC**: flow cytometry; **IF:** immunofluorescence; **FBS**: foetal bovine serum; **PB**: Phosphate buffer; **PBS**: phosphate buffer saline; **PFA:** paraformaldehyde; **kDa**: kiloDalton; **DAPI:** 4 ',6-diamino-2-fenilindol;

**Competing interests:** The authors declare that they have no competing interests.

## FIGURE LEGENDS

**Fig 1.- EGFP expression in Csf1r-EGFP transgenic mice.** Nuclei are stained with Dapi (blue); brain microglia/macrophages from direct fluorescence of Csf1r-EGFP cells (green), CD31 positive cells labeled blood vessel (red) and pan-laminin staining for basement membranes (white). (A, panel i), direct fluorescence map of adult mouse Csf1r-EGFP brain coronal sections (20x, 1.7x digital zoom). (B, panel i), showing 40X magnifications of EGFP-positive cells and CD31 positive cells in choroid plexus. Inset shows 63X (3x digital zoom) magnification of cells marked with an arrow. (C, panel i), 40X magnifications of EGFP-positive cells and CD31 positive cells in pia leptomeningeal membrane. Inset shows 63X (3x digital zoom) magnification of cells marked with an arrow. (A, panel ii); confocal microscopy z-stack images of 30 μm thick cryostat sections showing brain blood vessel marked with an arrow in panel i (63x, 3x digital zoom). Double asterisks (**) mark a parenchymal Csf1r-EGFP positive cells close to the blood vessel (juxtavascular) and green arrow marks a perivascular macrophage. Inset shows a 3D reconstruction of perivascular Csf1-EGFP positive cell. White arrows indicate both basement membranes (endothelial and parenchymal) around the Csf1-EGFP positive cell. (B, panel ii), confocal microscopy z-stack images of 30 μm thick cryostat sections, showing choroid plexus (63x, 3x digital zoom). (C. panel ii), confocal microscopy z-stack images of upper 30 μm from 80 μm vibratom sections showing pia leptomeningeal membranes (63x, 3x digital zoom). Insets in panels ii show 3D reconstructions of arrowed cells. Images were obtained with a SP5 Leica TCS confocal fluorescent microscope. Scale bars are included in the images. Images are representative of the different brain localizations.

**Fig 2.- Identification of CD45-positive brain cells.** Flow cytometry dot plots of live cells isolated from (A) brain except cerebellum and meningeal membranes and choroid plexus and (B) meningeal membranes and choroid plexus (m/Ch). Cells were isolated from wild type (WT) and Csf1r-EGFP mice, and stained with control isotype antibody (APC rat IgG2b; panel i) or with APC rat anti-mouse

CD45 (panels ii and iii). Panels iv show the arithmetic mean±SEM (n=5) of the percentage of $CD45^+$ (black) and $CD45^-$ (white) cells isolated. Panels v represent the arithmetic mean±SEM (n=5) of percentage of $EGFP^+$ cells in the Csf1r-EGFP cell isolates. The gating strategy was as presented in supplemental Fig 3s.

**Fig 3.- Analysis of $CD45^+$ cells from brain without m/Ch of WT C57BL6 mice treated with Flt3L.** (A) Mice were untreated (-Flt3L) or injected with B16 Flt3L-secreting tumor cells (+Flt3L), and myeloid isolates from brain w/o m/Ch (14 days post injection) were stained with APC rat anti-mouse CD45. $CD45^+$ cells were gated in both conditions. Bar graphs shows quantification of $CD45^+$ cells (black) as a percentage of total live cells in -Flt3L and +Flt3L mice. Bar graph shows the percentage of cells with high expression of CD45 ($CD45^h$) in -Flt3L versus +Flt3L mice. (B) Cells were doubled stained with APC rat anti-mouse CD45 together with Cy7-APC rat anti-mouse CD11b. $CD45^+CD11b^+$ brain parenchyma cells from Flt3L-treated mice can be separated into three subpopulations: $CD45^mCD11b^+$; $CD45^hCD11b^+$ and $CD45^hCD11b^{low}$. Histograms on the right show CD45, CD11b and CD11c staining on the surface of myeloid cells from brain w/o m/Ch: white histograms represent isotype control and black histograms represent specific staining with the antibodies indicated. (C) Numbers of $CD45^m$, $CD11b^+$ and $CD11b^{low}$ cells isolated (nº of cells/ 1000 $CD45^+$ brain parenchyma cells). The gating strategy was as presented in supplemental Fig 3s. Representative experiments or mean±SEM are shown of 7-8 independent experiments.

**Fig 4.- Analysis of $CD45^+$ cells from meningeal membranes and choroid plexus (m/Ch) of WT C57BL6 mice treated with Flt3L.** (A) Mice were untreated (-Flt3L) or injected with B16 Flt3L-secreting tumor cells (+Flt3L), and 14-d myeloid m/Ch isolates were stained with APC rat anti-mouse CD45. $CD45^+$ cells were gated in both conditions. Panel I shows quantification of $CD45^+$ cells (black) as a percentage of total live cells in -Flt3L and +Flt3L mice. (B) Cells were doubled stained with APC rat anti-mouse CD45 together with Cy7-APC rat anti-mouse CD11b. $CD45^+CD11b^+$ m/Ch cells from Flt3L-treated mice can be

separated into two subpopulations: $CD45^{h}CD11b^{+}$ and $CD45^{h}CD11b^{low}$. Histograms on the right show staining on the surface of CD45, CD11b and CD11c m/Ch myeloid cells: white histograms represent isotype control and black histograms represent specific staining with the antibodies indicated. (C) Numbers of $CD45^{m}$, $CD11b^{+}$ and $CD11b^{low}$ cells isolated (nº of cells/ 1000 $CD45^{+}$ m/Ch cells). Bar graph II on the far right of panel A shows $CD45^{h}CD11b^{low}$ (black) and $CD45^{h}CD11b^{+}$ (white) cells as a percentage of all $CD45^{+}$ cells isolated from -Flt3L and +Flt3L mice. The gating strategy was as presented in supplemental Fig 3s. Representative experiments are shown of 8 independent experiments, each consisting of pooled m/Ch preparations from two brains. Numerical data are presented as the mean±SEM of 7 independent experiments.

**Fig 5.- Expression of MHCII in the Flt3L-treated brain by Immunofluorescence.** Immunofluorescence staining of Csf1r-EGFP adult brain of adult mice treated with Flt3L (+Flt3L). 30 μm cryostat coronal brain sections (A, B and D) and 80 μm vibratome horizontal sections for meningeal membranes (C) were used. Sections were stained as follow: nuclei with Dapi (blue), microglia/macrophage visualized by direct fluorescence of Csf1r-EGFP (green), antibodies to mouse MCHII (red). In panel A, blood vessels were (C stained with pan-laminin (white) (A, panel i) 40x scan image of parenchymal brain, arrow indicates blood vessel amplified in panel ii. 40x scan image of choroid plexus (B, panel i) and pia leptomeningeal membrane (C, panel i); inset in panel C shows accumulation of $MHCII^{+}$ cells (red) in localized areas. Amplified areas shown in panel ii are marked with an arrow. (Panels ii) 63x amplification of the region marked (arrow) showing (A, panel ii). MHCII plus $CSF1R\text{-}EGFP^{+}$ and pan-laminin co-localization. Inset shows arrow-labelled MHCII positive cell (red). (B,panel ii) choroid plexus, insets show EGFP and MHCII staining separately. (C, panel ii), meningeal membrane, insets show EGFP and MHCII staining separately from arrow-marked cell. In panel B and C laminin staining was not shown. (D, panel i), 63x amplification of choroid plexus, shows negative control of tyramide enhanced IF method in choroid plexus. (D,

panel ii), co-staining of $CD11c^+$ cells (red), $MHCII^+$ cells (green) and nuclei with Dapi in blue. Individual staining is shown in left panels. Images were captured with a Leica SP5 TCS confocal microscope fitted with a 40x objective or a 63x objective with 3x digital zoom.

**Fig 6.- Expression of MHCII in the isolated brain cells from Flt3L-treated mouse.** WT male mice were Flt3L-treated. Flow cytometry dot plots of CD45/CD11b-positive cells in brain preparations as before(A) and m/Ch (B) from -Flt3L and +Flt3L animals (details as in Fig 3B and Fig 4B). Histograms show results of staining for MHCII with a FITC rat anti-mouse MHCII antibody. Dotted lines represent the fluorescence of the isotype control; gray histograms represent the specific staining. The percentage of MHCII-positive cells in each population is indicated as the mean±SEM of 3 independent experiments.

**Fig 7**. **Mouse *Dngr-1*/*Clec9a* gene structure and expression**. (A) *Dngr-1*/*Clec9a* gene structure, showing constituent exons and interspersing introns. The possible Dngr-1 protein variants are depicted underneath. The region amplified by real time PCR primers is indicated. (B) Expression of *Dngr-1* mRNA in spleen and different brain tissues (Ob: olfactory bulb, Cbl: cerebellum, CTX: cortex, Str: striatum, m/Ch: meninges/choroid plexus, SVZ: subventricular zone isolated as in (Ferron et al., 2007; Guo et al., 2012), Hpp: hippocampus, Th: thalamus). Samples were analysed by RT-PCR with primers for *Dngr-1*, with *β-actin* as the reference gene. Samples were loaded in equal quantities, except for spleen, which was loaded at a 1/30 relative dilution in order to avoid saturation due to the high expression in this tissue. Base-pair lengths of specific *Dngr-1* bands are indicated as follows: L corresponds to *Dngr-1* variant 1 (996 pb), S corresponds to variants 2 and 3 (918 and 915 pb) and VS to variant 4 (647 pb). (C) Mouse *Dngr-1* mRNA expression in spleen, m/Ch and brain preparationsof untreated (-) and Flt3L-treated (+) animals. *Dngr-1* specific mRNA was amplified from total mRNA using SYBR Green Real time PCR methodology; the reference sample was spleen from untreated animals and the reference gene was 36B4. **P≤ 0.01; * P≤0.05 for untreated (-) samples versus Flt3L-treated (+) samples (n=10).

**Fig 8.- DNGR-1-EGFP$^{+}$ cells in brain cell isolates.** Myeloid cells were analyzed from the brain as before (A) and m/Ch (B) of *Cle9a*$^{+/+}$ *wt* and *Cle9a* $^{egfp/egfp}$ littermates that were untreated (-Flt3L) or treated with Flt3L (+Flt3L) for 14 days. Flow cytometry dot plots show staining with APC rat anti-mouse CD45 antibody from a representative experiment of 5 performed. Gates are shown corresponding to total CD45$^{+}$ cells (dotted line) and CD45$^{+}$ cells with high intensity (CD45$^{h}$; dashed line). The oval regions demark the population of CD45$^{h}$ DNGR-1-EGFP$^{+}$ cells. Bar charts in A and B show numbers of CD45$^{h}$ DNGR-1-EGFP$^{+}$ cells per $10^{3}$ CD45$^{+}$ cells from control (-Flt3L) and treated (+Flt3L) animals. Data are mean±SEM of 5 independent experiments. To obtain sufficient cell numbers, m/Ch isolates from two brains were pooled for each condition.

**Fig 9.- MHCII expression in DNGR-1-EGFP$^{+}$ brain cells.** Flow cytometry dot plots of (A) myeloid (CD45$^{+}$) brain cells, and (B) CD45$^{+}$ m/Ch cells from Flt3L-treated *Cle9a*$^{egfp/egfp}$ mice. Cells were labeled with the following antibodies: PE-Cy7 rat anti-mouse CD45, Cy7-APC rat anti-mouse CD11b, and APC rat anti mouse MHCII (IA-IE). DNGR-1-EGFP$^{+}$ cells correspond to the CD45$^{h}$CD11b$^{low}$ subpopulation in isolates from brain w/o m/Ch (A) and m/Ch (B) (dotted line). Histograms show MHCII staining on the surface of CD45$^{h}$CD11b$^{low}$ DNGR-1-EGFP$^{+}$ cells in Flt3L-treated animals. Data are representative of three independent experiments performed. (C) IF analyses from Flt3L-treated *Cle9a*$^{egfp/egfp}$ mice choroid plexus; coronal brain sections were visualized by direct fluorescence of EGFP, and stained with antibodies to CD11c (Cy3 Tyramide) and MCHII (647 anti-rat). We show split channels of DNGR-1-EGFP+ cells marked with arrows. (D) RT-PCR analysis of *Dngr-1*, *Batf-3*, *Irf-8*, *Cd103*, *Cd80* and *Cd86* mRNA expression in m/Ch from control (-Flt3L) and treated (+Flt3L) mice. *** p<0.001 or ** p<0.01 with respect to m/Ch from control animals (n=6). (E) Batf-3$^{+/+}$ (WT) and Batf-3$^{-/-}$ mice littermates that were untreated (-Flt3L) or treated with Flt3L (+Flt3L) for 14 days. m/Ch isolated as before and *Dngr-1* specific mRNA was amplified from total mRNA using SYBR Green Real time PCR methodology; the reference sample was m/Ch from

untreated animals and the reference gene was 36B4. **P≤ 0.01; for untreated (-) samples versus Flt3L-treated (+) samples of n=4.

---

**Supplementary figures**

**Supplemental Fig 1s.- 3-D multichannel confocal reconstruction of meningeal myeloid cell visualization in Csf1r-EGFP mice.** 80 μm horizontal vibratome sections of Csf1r-EGFP mice pia leptomeningeal membranes were stained with antibodies to glial fibrillary acidic protein (GFAP) to stain astrocytes (red), and nuclei were stained with DAPI (blue). Myeloid cells were visualized by direct fluorescence of EGFP (green). Z-stack series (0.30 μm, 64, 62 μm in Z) were then acquired by confocal microcopy and processed by Image J, with high-level 3D visualization framework plugin for ImageJ*. Images were obtained with 63x magnification (3x digital zoom) in a SP5 Leica TCS confocal fluorescent microscope. Scale bars are included in the total image.

**Supplemental Fig 2s.- EGFP and Iba1 expression in steady-state adult brain of Csf1r-EGFP transgenic male mice.** Co-localization of representative Iba1 immunofluorescence (Wako) and CSF1R-EGFP direct fluorescence in 30 μm coronal cryostat sections of Csf1r-EGFP brain: (A) brain (B), choroid plexus, and 80 μm horizontal vibratome sections of (C) pia leptomeningeal membranes. Column i) shows Iba1 staining in red (Cy3) and nuclear staining in blue (DAPI). Column ii) shows EGFP direct fluorescence in green (EGFP) and nuclear staining in blue (DAPI). Column iii) shows merged fluorescence images of Iba1 in red (Cy3) and EGFP in green (EGFP). Images were obtained with a Leica SP5 TCS confocal microscope, with 40x (main panels) and 63x (insets) air objectives. 63x views were taken with 3x digital zoom, and show the cells marked with an asterisk in the main panels. Scale bars are included in the images. Images are representative of at least 4 different preparations. The percentage of $Iba1^+$ $CSF1R\text{-}EGFP^+$ cells in each brain area is indicated as the mean±SEM of n=4 independent animals. In the meningeal preparation, CSF1R-

EGFP$^+$ evaluated were those situated in the first 30 μm of the 80 μm horizontal vibratom sections.

**Supplemental Fig 3s.- Gating strategy for flow cytometry analysis:** Cells were obtained and labeled as described in Materials and Methods from brain without m/Ch(A) and from m/Ch (B). Before flow cytometry analysis, propidium iodide (PI; 0.5 μg/ml) was added to determine cell viability. Cells were first gated (P1) on the basis of size and complexity (SSC vs FSC). Doublet discrimination was performed by FSC-H vs FSC-W and SSC-H vs SSC-W analyses, and then PI negative cells (i.e. live cells) were selected for further analysis.

**Supplemental Fig 4s.- DNGR-1-EGFP expression in the spleen of *Clec9a*$^{+/+}$ *WT mice and Clec9a*$^{egfp/egfp}$ *mice.*** *Clec9a*$^{+/+}$ *WT mice and Cle9a*$^{egfp/egfp}$ mice were treated with Flt3L for 14 days, and splenocytes were isolated as described in Material and Methods. Spleen cells were stained with PE-Cy7 Armenian hamster anti-mouse CD11c or the control isotype. CD11c$^+$ DNGR-1-EGFP$^+$ cells were identified and further analyzed with APC-rat anti mouse CD45, APC-Cy7 rat anti-mouse CD11b, PE-Cy7 Armenian hamster anti-mouse CD11c antibodies and APC rat anti mouse MHCII (IA-IE). Histograms represent the expression of the DNGR-1-EGFP$^+$ (EGFP), CD11b, CD45 CD11c (panel B) and MHCII (panel C) in splenocytes. Isotype controls are represented by the dotted lines. Data is a representative experiment of 5 different experiments done. These animals were used for the identification of myeloid brain cells and m/Ch cells analyzed in Fig 7.

Figures Reviewed

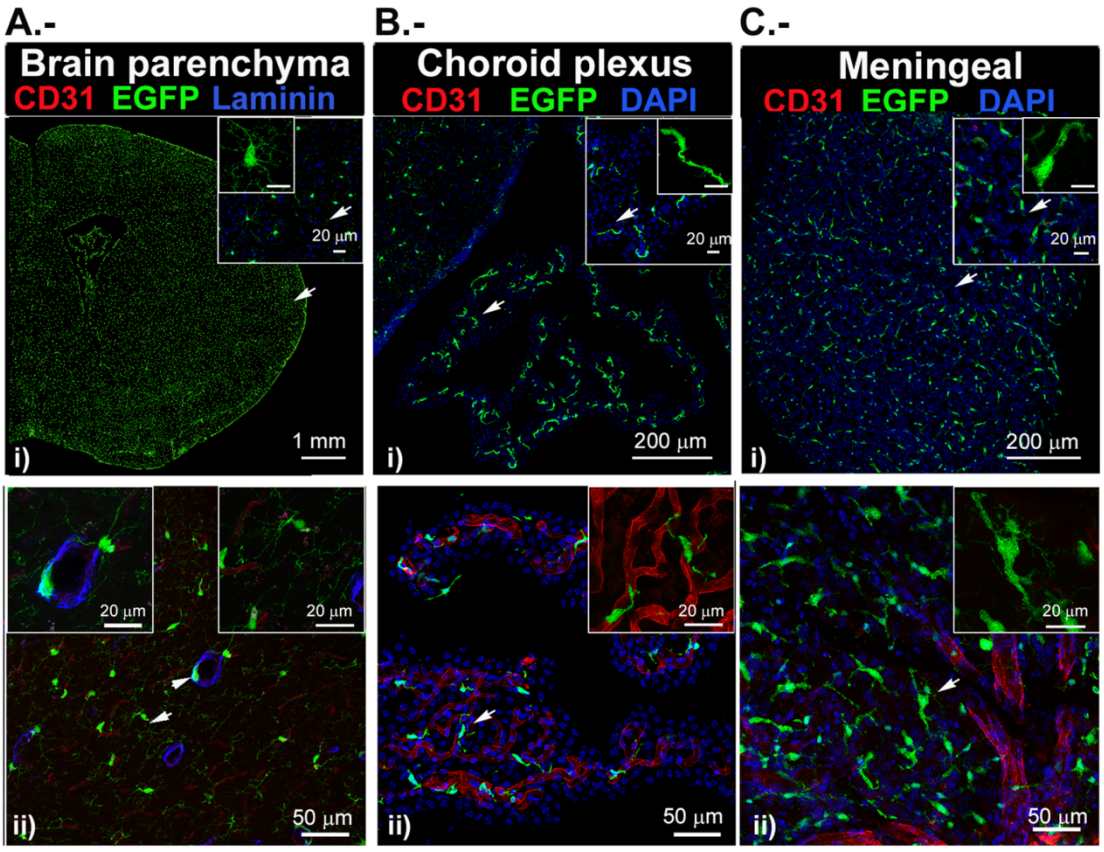

Fig 2

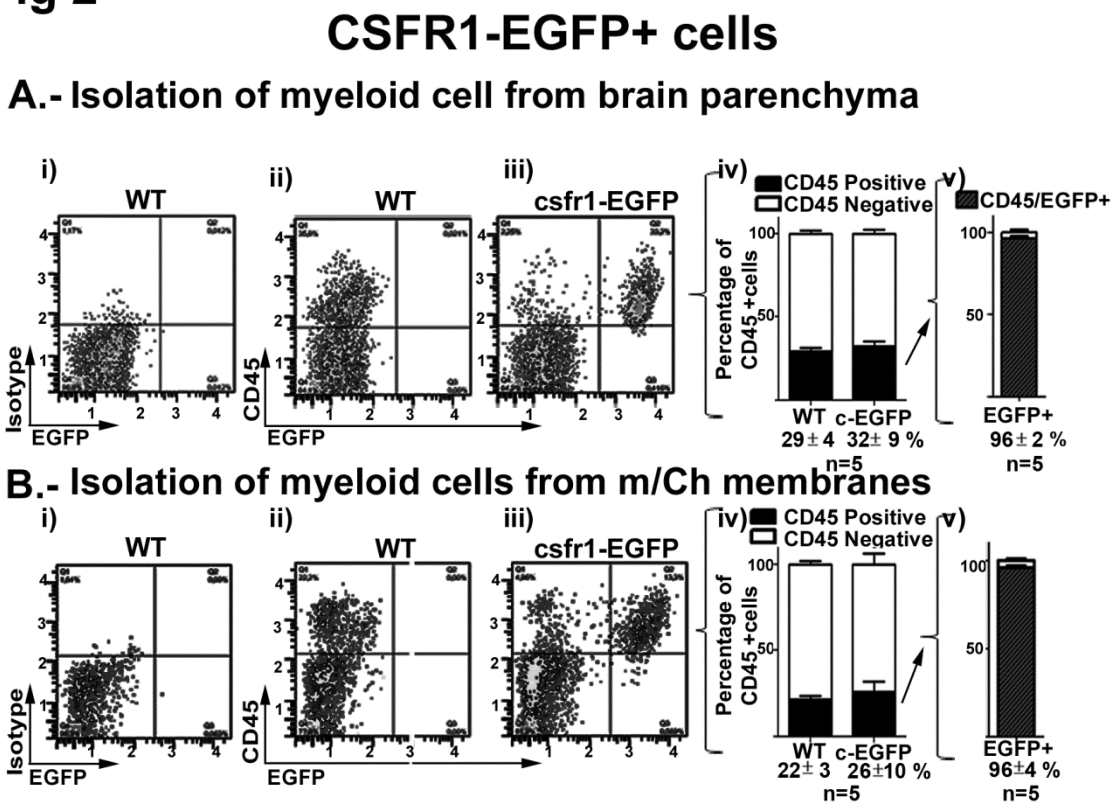

# Fig 3

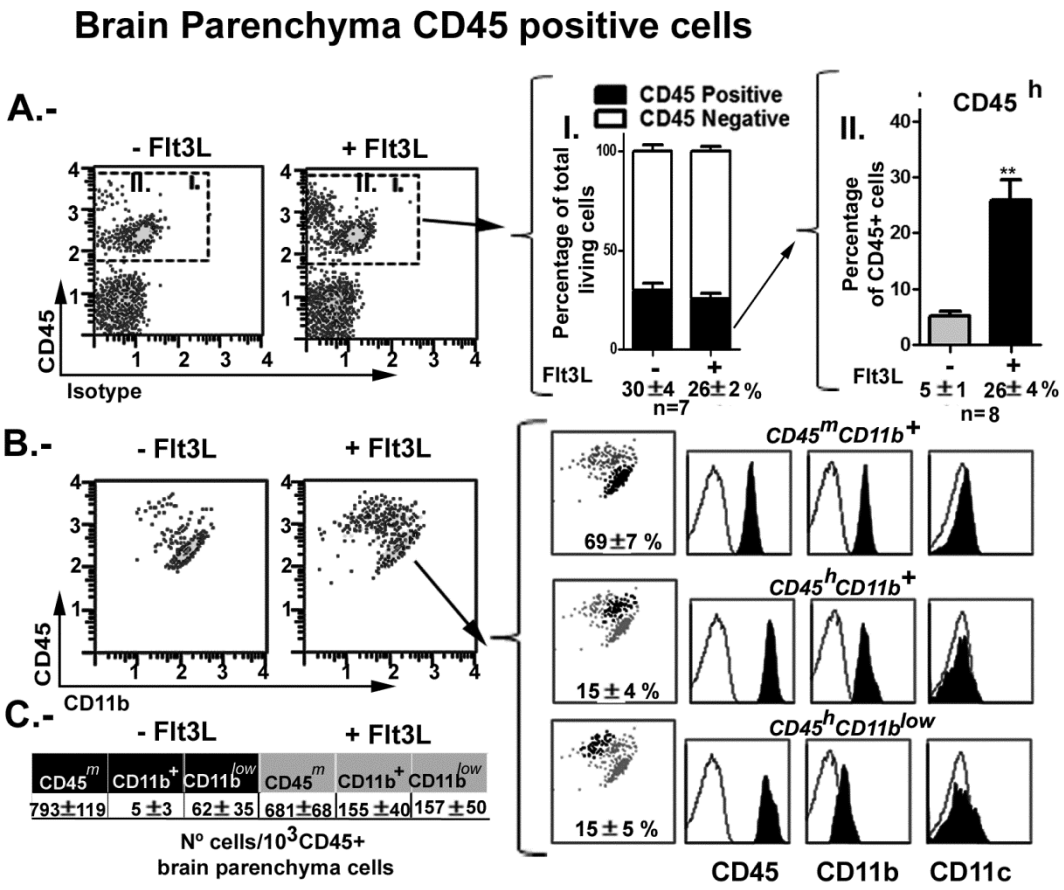

# Fig 4

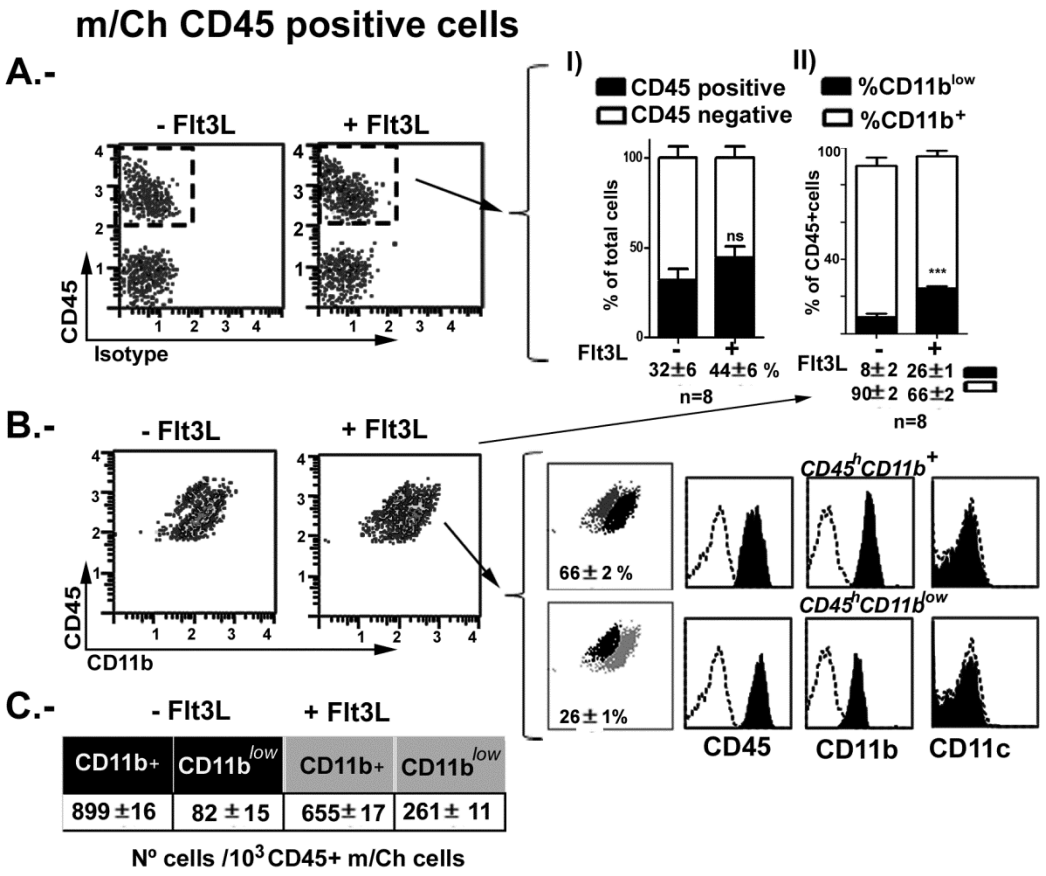

Fig 5

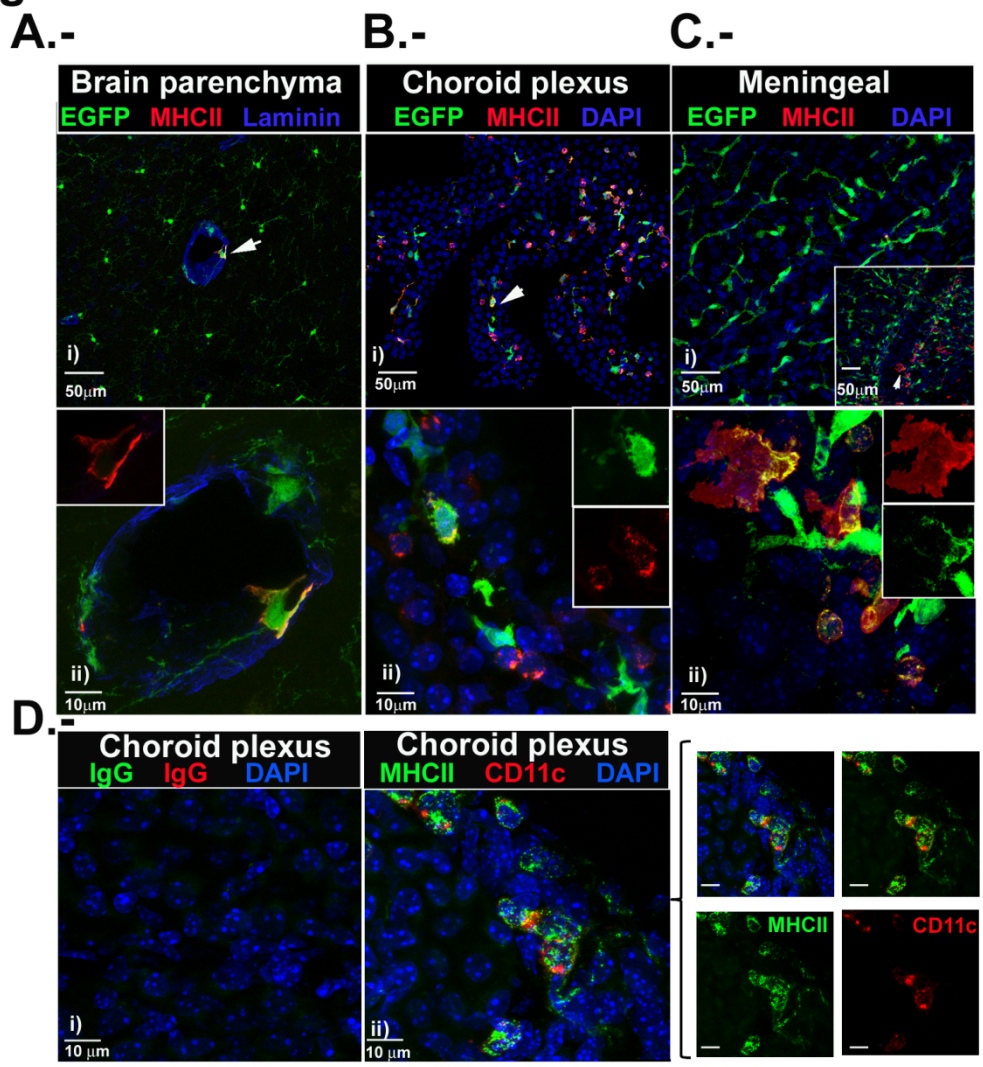


Fig 6

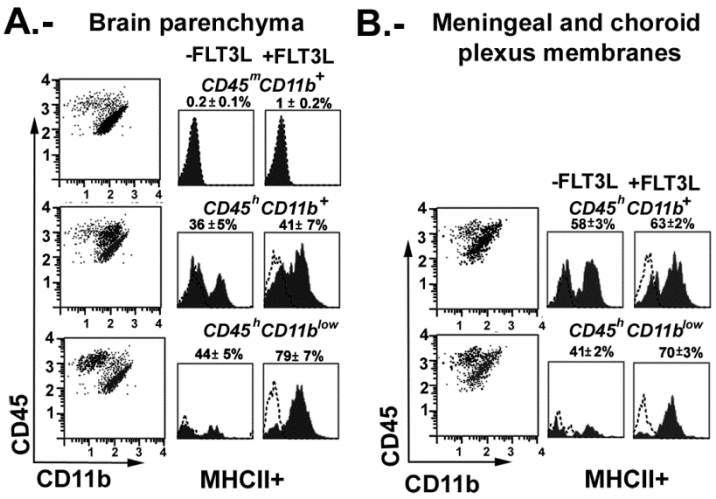

# Fig 7

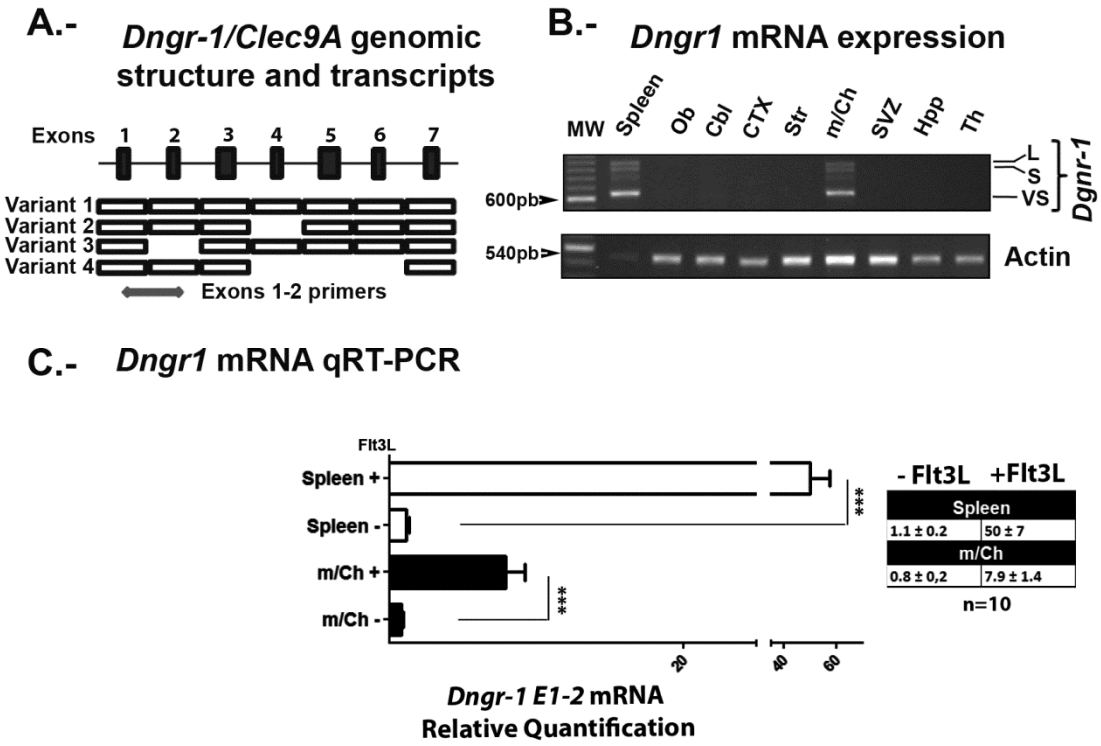

# Fig 8

## A.- Brain Parenchyma

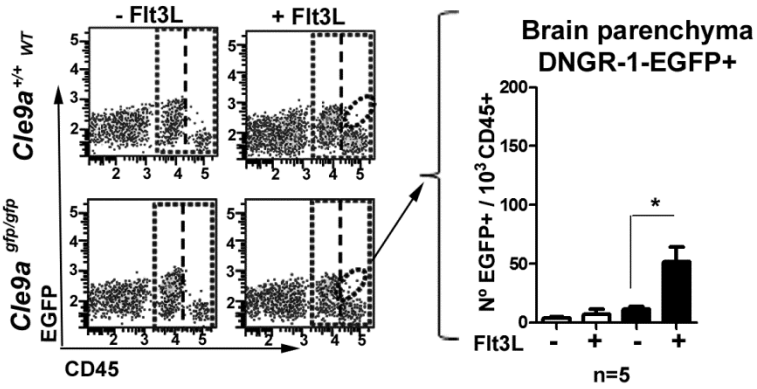


## B.- m/Ch

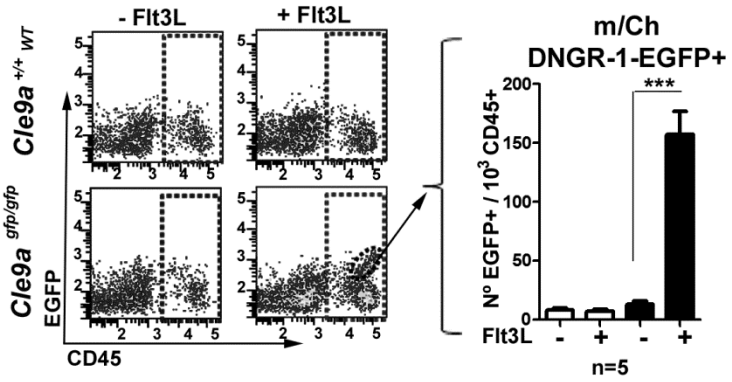

# Fig 9

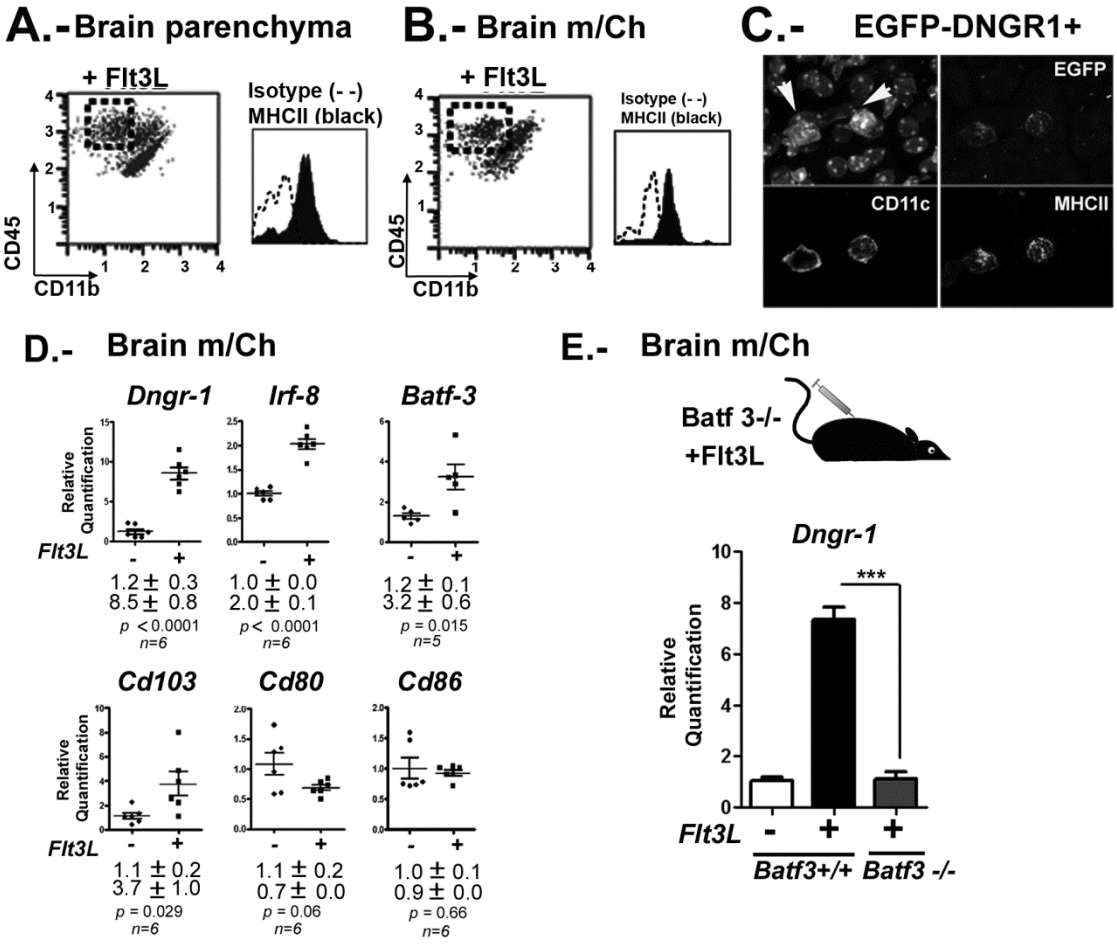

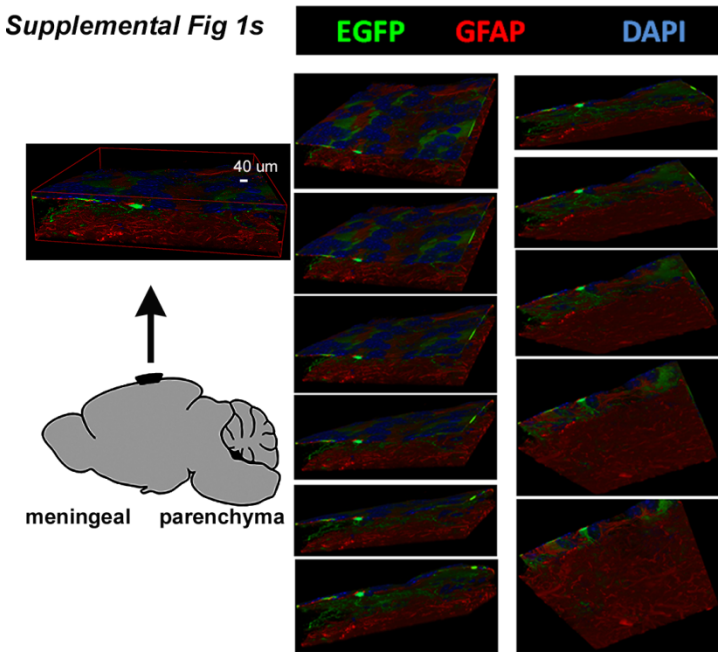

## supplemental figure 2s

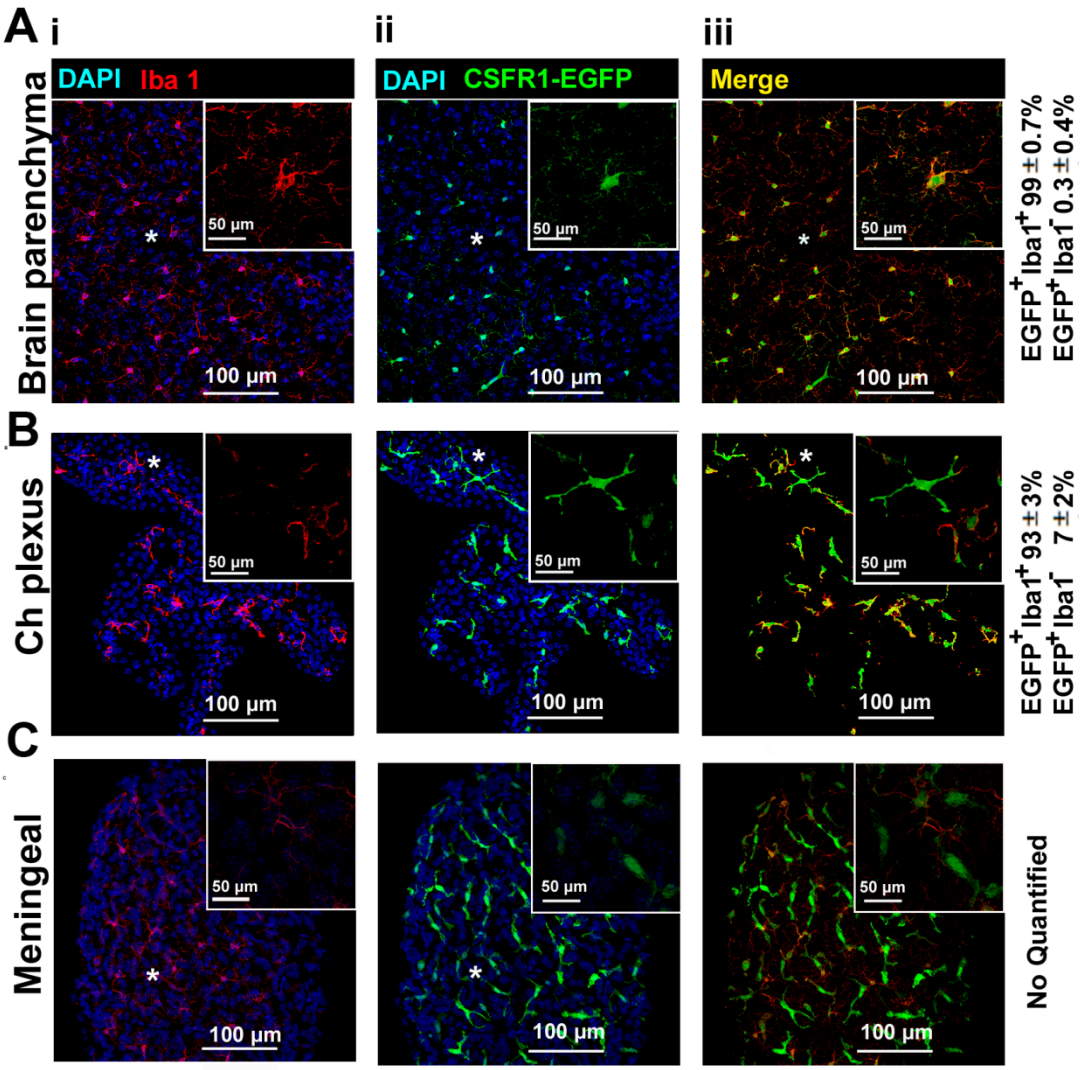

## Supplemental Figure 3s

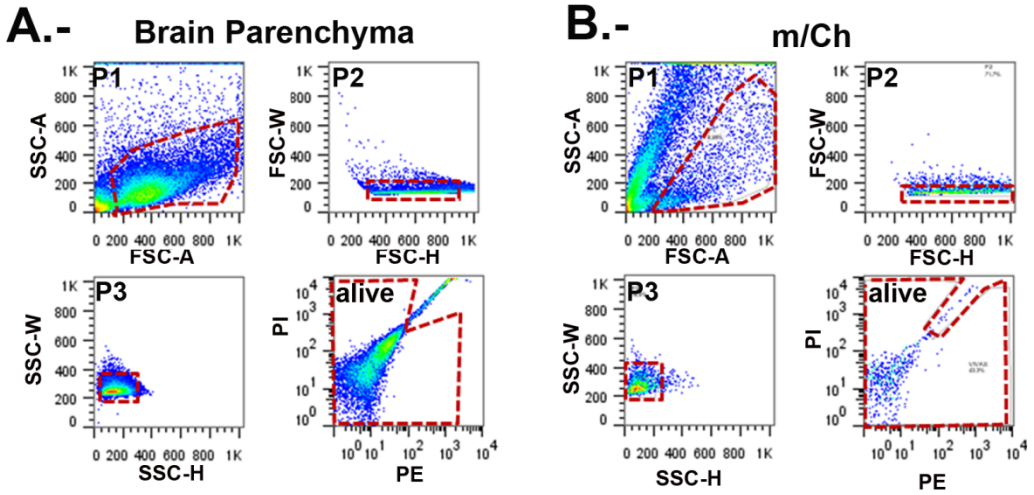


## Supplemental Figure 4s

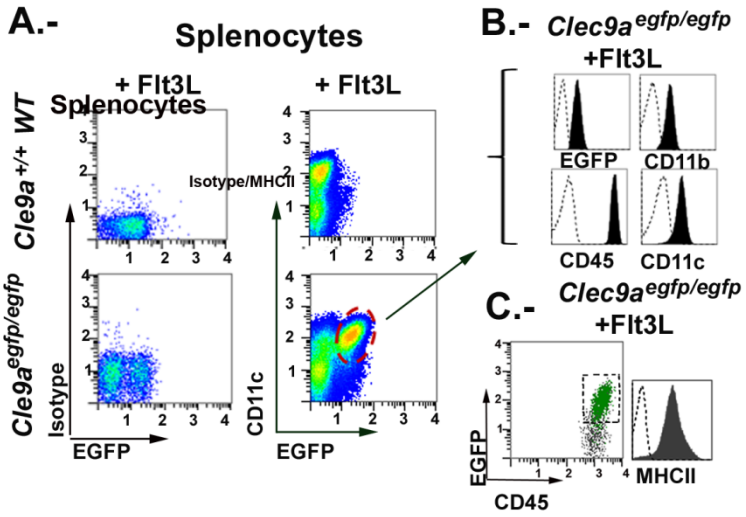


*Reference List*

*Ajami B, Bennett JL, Krieger C, Tetzlaff W, Rossi FM. 2007. Local self-renewal can sustain CNS microglia maintenance and function throughout adult life. Nat Neurosci 10:1538-1543.*

*Anandasabapathy N, Victora GD, Meredith M, Feder R, Dong B, Kluger C, Yao K, Dustin ML, Nussenzweig MC, Steinman RM, Liu K. 2011. Flt3L controls the development of radiosensitive dendritic cells in the meninges and choroid plexus of the steady-state mouse brain. J Exp Med 208:1695-1705.*

*Axtell RC, Steinman L. 2009. Gaining entry to an uninflamed brain. Nat Immunol 10:453-455.*

*Bulloch K, Miller MM, Gal-Toth J, Milner TA, Gottfried-Blackmore A, Waters EM, Kaunzner UW, Liu K, Lindquist R, Nussenzweig MC, Steinman RM, McEwen BS. 2008. CD11c/EYFP transgene illuminates a discrete network of dendritic cells within the embryonic, neonatal, adult, and injured mouse brain. J Comp Neurol 508:687-710.*

*Caminschi I, Lahoud MH, Shortman K. 2009. Enhancing immune responses by targeting antigen to DC. Eur J Immunol 39:931-938.*

*Caminschi I, Proietto AI, Ahmet F, Kitsoulis S, Shin TJ, Lo JC, Rizzitelli A, Wu L, Vremec D, van Dommelen SL, Campbell IK, Maraskovsky E, Braley H, Davey GM, Mottram P, van d, V, Jensen K, Lew AM, Wright MD, Heath WR, Shortman K, Lahoud MH. 2008. The dendritic cell subtype-restricted C-type lectin Clec9A is a target for vaccine enhancement. Blood 112:3264-3273.*

*Carson MJ, Reilly CR, Sutcliffe JG, Lo D. 1998. Mature microglia resemble immature antigen-presenting cells. Glia 22:72-85.*

*D'Agostino PM, Gottfried-Blackmore A, Anandasabapathy N, Bulloch K. 2012. Brain dendritic cells: biology and pathology. Acta Neuropathol 124:599-614.*

*del Rio ML, Bernhardt G, Rodriguez-Barbosa JI, Forster R. 2010. Development and functional specialization of CD103+ dendritic cells. Immunol Rev 234:268-281.*

*Elmore MR, Najafi AR, Koike MA, Dagher NN, Spangenberg EE, Rice RA, Kitazawa M, Matusow B, Nguyen H, West BL, Green KN. 2014. Colony-stimulating factor 1 receptor signaling is necessary for microglia viability, unmasking a microglia progenitor cell in the adult brain. Neuron 82:380-397.*

*Engelhardt B, Ransohoff RM. 2005. The ins and outs of T-lymphocyte trafficking to the CNS: anatomical sites and molecular mechanisms. Trends Immunol 26:485-495.*

*Erblich B, Zhu L, Etgen AM, Dobrenis K, Pollard JW. 2011. Absence of colony stimulation factor-1 receptor results in loss of microglia, disrupted brain development and olfactory deficits. PLoS One 6:e26317.*

*Ferron SR, Andreu-Agullo C, Mira H, Sanchez P, Marques-Torrejon MA, Farinas I. 2007. A combined ex/in vivo assay to detect effects of exogenously added factors in neural stem cells. Nat Protoc 2:849-859.*

*Fischer HG, Reichmann G. 2001. Brain dendritic cells and macrophages/microglia in central nervous system inflammation. J Immunol 166:2717-2726.*

*Ford AL, Goodsall AL, Hickey WF, Sedgwick JD. 1995. Normal adult ramified microglia separated from other central nervous system macrophages by flow cytometric sorting. Phenotypic differences defined and direct ex vivo antigen presentation to myelin basic protein-reactive CD4+ T cells compared. J Immunol 154:4309-4321.*

*Galea I, Bechmann I, Perry VH. 2007. What is immune privilege (not)? Trends Immunol 28:12-18.*

*Ginhoux F, Greter M, Leboeuf M, Nandi S, See P, Gokhan S, Mehler MF, Conway SJ, Ng LG, Stanley ER, Samokhvalov IM, Merad M. 2010. Fate mapping analysis reveals that adult microglia derive from primitive macrophages. Science 330:841-845.*

*Ginhoux F, Liu K, Helft J, Bogunovic M, Greter M, Hashimoto D, Price J, Yin N, Bromberg J, Lira SA, Stanley ER, Nussenzweig M, Merad M. 2009. The origin and development of nonlymphoid tissue CD103+ DCs. J Exp Med 206:3115-3130.*

*Greter M, Heppner FL, Lemos MP, Odermatt BM, Goebels N, Laufer T, Noelle RJ, Becher B. 2005. Dendritic cells permit immune invasion of the CNS in an animal model of multiple sclerosis. Nat Med 11:328-334.*

*Guo W,Patzlaff NE,Jobe EM, Zhao X. Microdissection of the SVZ and the DG of a single adult mouse. Isolation of multipotent neural stem or progenitor cells from both the dentate gyrus and subventricular zone of a single adult mouse. Nature Protocols 7, 2005–2012 (2012).*

*Heath WR, Carbone FR. 2009. Dendritic cell subsets in primary and secondary T cell responses at body surfaces. Nat Immunol 10:1237-1244.*

*Hickey WF. 2001. Basic principles of immunological surveillance of the normal central nervous system. Glia 36:118-124.*

*Hildner K, Edelson BT, Purtha WE, Diamond M, Matsushita H, Kohyama M, Calderon B, Schraml BU, Unanue ER, Diamond MS, Schreiber RD, Murphy TL, Murphy KM. 2008. Batf3 deficiency reveals a critical role for CD8alpha+ dendritic cells in cytotoxic T cell immunity. Science 322:1097-1100.*

*Huysamen C, Brown GD. 2009. The fungal pattern recognition receptor, Dectin-1, and the associated cluster of C-type lectin-like receptors. FEMS Microbiol Lett 290:121-128.*

*Huysamen C, Willment JA, Dennehy KM, Brown GD. 2008. CLEC9A is a novel activation C-type lectin-like receptor expressed on BDCA3+ dendritic cells and a subset of monocytes. J Biol Chem 283:16693-16701.*

*Iborra S, Izquierdo HM, Martinez-Lopez M, Blanco-Menendez N, Reis e Sousa, Sancho D. 2012. The DC receptor DNGR-1 mediates cross-priming of CTLs during vaccinia virus infection in mice. J Clin Invest 122:1628-1643.*

*Immig K, Gericke M, Menzel F, Merz F, Krueger M, Schiefenhovel F, Losche A, Jager K, Hanisch UK, Biber K, Bechmann I. 2015. CD11c-positive cells from brain, spleen, lung, and liver exhibit site-specific immune phenotypes and plastically adapt to new environments. Glia 63:611-625.*

*Inaba K, Turley S, Yamaide F, Iyoda T, Mahnke K, Inaba M, Pack M, Subklewe M, Sauter B, Sheff D, Albert M, Bhardwaj N, Mellman I, Steinman RM. 1998. Efficient presentation of phagocytosed cellular fragments on the major histocompatibility complex class II products of dendritic cells. J Exp Med 188:2163-2173.*

*Ito D, Imai Y, Ohsawa K, Nakajima K, Fukuuchi Y, Kohsaka S. 1998. Microglia-specific localisation of a novel calcium binding protein, Iba1. Brain Res Mol Brain Res 57:1-9.*

*Iyoda T, Inaba K. 2002. [Immune regulation by dendritic cells]. Tanpakushitsu Kakusan Koso 47:2133-2138.*

*Jung S, Unutmaz D, Wong P, Sano G, De los SK, Sparwasser T, Wu S, Vuthoori S, Ko K, Zavala F, Pamer EG, Littman DR, Lang RA. 2002. In vivo depletion of CD11c+ dendritic cells abrogates priming of CD8+ T cells by exogenous cell-associated antigens. Immunity 17:211-220.*

*Karman J, Chu HH, Co DO, Seroogy CM, Sandor M, Fabry Z. 2006. Dendritic cells amplify T cell-mediated immune responses in the central nervous system. J Immunol 177:7750-7760.*

*Lindquist RL, Shakhar G, Dudziak D, Wardemann H, Eisenreich T, Dustin ML, Nussenzweig MC. 2004. Visualizing dendritic cell networks in vivo. Nat Immunol 5:1243-1250.*

*Livak KJ, Schmittgen TD. 2001. Analysis of relative gene expression data using real-time quantitative PCR and the 2(-Delta Delta C(T)) Method. Methods 25:402-408.*

*Lv M, Liu Y, Zhang J, Sun L, Liu Z, Zhang S, Wang B, Su D, Su Z. 2011. Roles of inflammation response in microglia cell through Toll-like receptors 2/interleukin-23/interleukin-17 pathway in cerebral ischemia/reperfusion injury. Neuroscience 176:162-172.*

*Matyszak MK, Lawson LJ, Perry VH, Gordon S. 1992. Stromal macrophages of the choroid plexus situated at an interface between the brain and peripheral immune system constitutively express major histocompatibility class II antigens. J Neuroimmunol 40:173-181.*

*Matyszak MK, Perry VH. 1996. The potential role of dendritic cells in immune-mediated inflammatory diseases in the central nervous system. Neuroscience 74:599-608.*

*McMahon EJ, Bailey SL, Castenada CV, Waldner H, Miller SD. 2005. Epitope spreading initiates in the CNS in two mouse models of multiple sclerosis. Nat Med 11:335-339.*

*McMenamin PG. 1999. Distribution and phenotype of dendritic cells and resident tissue macrophages in the dura mater, leptomeninges, and choroid plexus of the rat brain as demonstrated in wholemount preparations. J Comp Neurol 405:553-562.*

*McMenamin PG, Wealthall RJ, Deverall M, Cooper SJ, Griffin B. 2003. Macrophages and dendritic cells in the rat meninges and choroid plexus: three-dimensional localisation by environmental scanning electron microscopy and confocal microscopy. Cell Tissue Res 313:259-269.*

*Mildner A, Schmidt H, Nitsche M, Merkler D, Hanisch UK, Mack M, Heikenwalder M, Bruck W, Priller J, Prinz M. 2007. Microglia in the adult brain arise from Ly-6ChiCCR2+ monocytes only under defined host conditions. Nat Neurosci 10:1544-1553.*

*Murphy KM. 2013. Transcriptional control of dendritic cell development. Adv Immunol 120:239-267.*

*Nimmerjahn A, Kirchhoff F, Helmchen F. 2005. Resting microglial cells are highly dynamic surveillants of brain parenchyma in vivo. Science 308:1314-1318.*

*Pashenkov M, Teleshova N, Link H. 2003. Inflammation in the central nervous system: the role for dendritic cells. Brain Pathol 13:23-33.*

*Piva L, Tetlak P, Claser C, Karjalainen K, Renia L, Ruedl C. 2012. Cutting edge: Clec9A+ dendritic cells mediate the development of experimental cerebral malaria. J Immunol 189:1128-1132.*

*Pooley JL, Heath WR, Shortman K. 2001. Cutting edge: intravenous soluble antigen is presented to CD4 T cells by CD8- dendritic cells, but cross-presented to CD8 T cells by CD8+ dendritic cells. J Immunol 166:5327-5330.*

*Poulin LF, Reyal Y, Uronen-Hansson H, Schraml BU, Sancho D, Murphy KM, Hakansson UK, Moita LF, Agace WW, Bonnet D, Reis e Sousa. 2012. DNGR-1 is a specific and universal marker of mouse and human Batf3-dependent dendritic cells in lymphoid and nonlymphoid tissues. Blood 119:6052-6062.*

*Poulin LF, Salio M, Griessinger E, Anjos-Afonso F, Craciun L, Chen JL, Keller AM, Joffre O, Zelenay S, Nye E, Le Moine A, Faure F, Donckier V, Sancho D, Cerundolo V, Bonnet D, Reis e Sousa. 2010. Characterization of human DNGR-1+ BDCA3+ leukocytes as putative equivalents of mouse CD8alpha+ dendritic cells. J Exp Med 207:1261-1271.*

*Prinz M, Tay TL, Wolf Y, Jung S. 2014. Microglia: unique and common features with other tissue macrophages. Acta Neuropathol 128:319-331.*

*Probst HC, Tschannen K, Odermatt B, Schwendener R, Zinkernagel RM, van den Broek M. 2005. Histological analysis of CD11c-DTR/GFP mice after in vivo depletion of dendritic cells. Clin Exp Immunol 141:398-404.*

*Prodinger C, Bunse J, Kruger M, Schiefenhovel F, Brandt C, Laman JD, Greter M, Immig K, Heppner F, Becher B, Bechmann I. 2011. CD11c-expressing cells reside in the juxtavascular parenchyma and extend processes into the glia limitans of the mouse nervous system. Acta Neuropathol 121:445-458.*

*Puntener U, Booth SG, Perry VH, Teeling JL. 2012. Long-term impact of systemic bacterial infection on the cerebral vasculature and microglia. J Neuroinflammation 9:146.*

*Ransohoff RM, Cardona AE. 2010. The myeloid cells of the central nervous system parenchyma. Nature 468:253-262.*

*Ransohoff RM, Engelhardt B. 2012. The anatomical and cellular basis of immune surveillance in the central nervous system. Nat Rev Immunol 12:623-635.*

*Sancho D, Joffre OP, Keller AM, Rogers NC, Martinez D, Hernanz-Falcon P, Rosewell I, Reis e Sousa. 2009. Identification of a dendritic cell receptor that couples sensing of necrosis to immunity. Nature 458:899-903.*

*Sancho D, Mourao-Sa D, Joffre OP, Schulz O, Rogers NC, Pennington DJ, Carlyle JR, Reis e Sousa. 2008. Tumor therapy in mice via antigen targeting to a novel, DC-restricted C-type lectin. J Clin Invest 118:2098-2110.*

*Sasmono RT, Oceandy D, Pollard JW, Tong W, Pavli P, Wainwright BJ, Ostrowski MC, Himes SR, Hume DA. 2003. A macrophage colony-stimulating factor receptor-green fluorescent protein transgene is expressed throughout the mononuclear phagocyte system of the mouse. Blood 101:1155-1163.*

*Schraml BU, van BJ, Zelenay S, Whitney PG, Filby A, Acton SE, Rogers NC, Moncaut N, Carvajal JJ, Reis e Sousa. 2013. Genetic tracing via DNGR-1 expression history defines dendritic cells as a hematopoietic lineage. Cell 154:843-858.*

*Schulz O, Reis e Sousa. 2002. Cross-presentation of cell-associated antigens by CD8alpha+ dendritic cells is attributable to their ability to internalize dead cells. Immunology 107:183-189.*

*Serafini B, Columba-Cabezas S, Di RF, Aloisi F. 2000. Intracerebral recruitment and maturation of dendritic cells in the onset and progression of experimental autoimmune encephalomyelitis. Am J Pathol 157:1991-2002.*

*Serrano-Perez MC, Martin ED, Vaquero CF, Azcoitia I, Calvo S, Cano E, Tranque P. 2011. Response of transcription factor NFATc3 to excitotoxic and traumatic brain insults: identification of a subpopulation of reactive astrocytes. Glia 59:94-107.*

*Shechter R, London A, Schwartz M. 2013. Orchestrated leukocyte recruitment to immune-privileged sites: absolute barriers versus educational gates. Nat Rev Immunol 13:206-218.*

*Shortman K, Heath WR. 2010. The CD8+ dendritic cell subset. Immunol Rev 234:18-31.*

*van Rijt LS, Jung S, KleinJan A, Vos N, Willart M, Duez C, Hoogsteden HC, Lambrecht BN. 2005. In vivo depletion of lung CD11c+ dendritic cells during allergen challenge abrogates the characteristic features of asthma. J Exp Med 201:981-991.*

*Watowich SS, Liu YJ. 2010. Mechanisms regulating dendritic cell specification and development. Immunol Rev 238:76-92.*

*Zelenay S, Keller AM, Whitney PG, Schraml BU, Deddouche S, Rogers NC, Schulz O, Sancho D, Reis e Sousa. 2012. The dendritic cell receptor DNGR-1 controls endocytic handling of necrotic cell antigens to favor cross-priming of CTLs in virus-infected mice. J Clin Invest 122:1615-1627.*